Kinetic Modeling of Batch Reaction Processes

David Joiner

September, 2012

Director of Thesis: Dr. Paul J. Gemperline

Major Department: Chemistry

Kinetic models have been demonstrated to be useful in on-line batch monitoring systems. The ability to monitor a reaction in real time is invaluable to the production process of industrial and pharmaceutical products. However, it is not a commonly used technique, due to some of its limitations. Currently, a great deal of work has been done showing the ability of a kinetic model to accurately estimate the spectral profiles and concentrations of reaction systems as a function of time. Some models have even demonstrated the technique's ability to model the transitions of analytes during dissolution and crystallization processes, but little has been done to combine all of these processes into a flexible, robust modeling system that incorporates all of these processes simultaneously.

The goal of this work is three-fold: (1) to demonstrate the ability of a kinetic model to cohesively model dissolution, reaction, and crystallization processes, (2) accurately predict the spectral and concentration information produced by the reaction system, and (3), to accurately model an actual industrial slurry reaction using these same methods.

For first part of this work, an acetylsalicylic acid synthesis model system was chosen. This synthesis reaction contains all of the processes necessary to produce a cohesive model

including dissolution of the salicylic acid reactant, simultaneous reaction of the reactants to form the product and side products, and subsequent crystallization and precipitation of the product. This work was performed using ATR-UV/Vis measurements to model changes in the solution phase of the reaction mixture and utilized HPLC measurements for validation of the results.

The second part of this work used the same techniques seen in part one and extended them to a complex industrial slurry model system. This section of the work was performed using NIR reflectance measurements to model the changes in the solid phase of the reaction mixture. This portion also used HPLC measurements for validation purposes.

The work done within these two sections demonstrates the ability of the kinetic model to operate in both in the solid and liquid state and using multiple spectroscopic methods.

Kinetic Modeling of Batch Reaction Processes

A Thesis

Presented to the Faculty of the Department of Chemistry

East Carolina University

For Partial Fulfillment of the Requirements for the Degree

Master of Science in Chemistry

by

David Joiner

November, 2012

Kinetic Modeling of Batch Reaction Processes

By

David Joiner

Approved by:

Director of Thesis: _____
Paul J. Gemperline, PhD

Committee Member: _____
Anthony Kennedy, PhD

Committee Member: _____
Yu Yang, PhD

Committee Member: _____
Mary Ellen McNally, PhD

Chair of the Department of Chemistry:

_____
Ricky P. Hicks, PhD

Dean of the Graduate School:

_____
Paul J. Gemperline, PhD

Acknowledgements:

First, I would like to thank my advisor and mentor Dr. Paul Gemperline. After allowing me to work in his lab for two years as an undergraduate (and break a few expensive things), he was brave enough to let me come back and continue doing research in his lab as a graduate student (where I broke a few more expensive things). His knowledge and enthusiasm for science was truly inspiring and I could not have asked for a better mentor and friend to help guide me through my graduate career. I would also like to thank my committee members Dr. Anthony Kennedy, Dr. Yu Yang, and Dr. Mary Ellen McNally for their advice and criticisms of my work. Their advice was invaluable to getting this work to where it is today. I would also like to thank Dr. Julien Billeter, for spending the time to teach me the basics, and for spending at least a couple very, very late nights working with me to meet deadlines. These actions are a testament to his patience and devotion to his work. I would like to thank the National Science Foundation (NSF) under grant number CHE-0750287 for Grant Opportunities for Academic Liaison with Industry (GOALI) and E.I. DuPont de Nemours and Co., Inc., Crop Protection Products and Engineering Technologies for their funding of this research. I also would like to thank the principal investigators on this project, Dr. Ron Hoffman (DuPont), Dr. Frank Chambers (OSU), Dr. Liguo Song (UTK), and Dr. Kelsey Cook (NSF), for their advice and questions that helped to push this work forward. I would also like to thank all of the people, both new and old, that worked in our lab and helped me to grow as a scientist and as a person, in particular, Mr. Chun Hsieh, Ms. Tess Kirchner, Mr. John Blanton, Mr. Chad Adkins, Mr. Ethan Chiappisi, and Ms. Kristian Scott. Next, I would like to thank my beautiful fiancé, Ms. Olivia Fairchild, for providing me with love and support throughout my research and for giving me the occasional kick in the

rear when I chose to nap instead of write. I love you. Most of all I would like to thank my parents, Jimmy and Audrey Joiner, for pushing me to give my best effort in all things I do, for guiding me through life, and always being available to give advice, listen to me complain, or tell me I need to get my oil changed. It is because of you that I grew into the person I am today, and I could not have asked for two better people to be my parents. I love you both very much.

Table of Contents

Table of Figures

1. Introduction

Notes on the organization of this thesis: Chapter 1 provides a basic introduction to the research material and Chapter 2 provides theory and background for the techniques that were used in this work. Chapters 3 and 4 are manuscripts for publication detailing the results of this work. Since these chapters are presented in the form of a research article manuscript, much of the information in Chapters 1 and 2 of this thesis will be repeated in the early portions of Chapters 3 and 4, albeit in less detail. Chapter 4 was written in collaboration with another author, Chun Hsieh. The author of this work wrote the Introduction and Theory sections of Chapter 4 and Section 4.3.4. The author of this thesis performed the Partial Least Squares Regression modeling which was used to confirm the viability of modeling a commercial slurry system, shown in Section 4.3.4. The kinetic modeling results shown in Chapter 4 are from the work of Chun Hsieh and Dr. Paul Gemperline.

In an industrial setting, it is necessary to have a complete understanding of every reaction process that takes place in a production facility. Optimizing a reaction in order to save on the cost of materials and establishing safety guidelines in order to protect employees and facilities are a couple of the reasons that this knowledge is needed. Mistakes in production can be very costly, and the use of preventative measures can be very beneficial to a manufacturing process. An active area of research involves the development of “kinetic models”. These models have the ability to mathematically explain all of the crucial processes that are taking place within a particular reaction system. These models are supplemented by the use of

spectroscopic measurement techniques that can be be used to monitor a reaction in an industrial setting in real time. This “batch reaction monitoring” is very useful and can be used as a preventative measure for mistakes in the manufacturing process[1, 2].

At the moment, kinetic modeling in industry is not the norm. Currently, Partial Least Squares (PLS) regression modeling is the most frequently used form of modeling industrial reactions[1, 3-5]. PLS is very good at monitoring specific reaction protocols and the technique is be very robust; but, these types of models can be very reaction specific and are not always good at adjusting to changes in the reaction formulation or changes in the production methods. To build a PLS model, a large number of datasets from very similar experiments are assembled and used as a model for how the system should behave. However, if the original protocol is significantly changed, then a new PLS model may need to be constructed in order to fit the new experimental protocol. The PLS model may not always adequately predict the outcome of a reaction if a significant change has been made to the reaction components. For instance, customer requested changes in a product formulation similar to one already in production with an already viable PLS model may invalidate the ability of the PLS model to predict accurate concentrations. Building a new model for a different formulation can be incredibly time consuming and may not be considered financially beneficial. The form of kinetic modeling presented in this work can be more adaptable, in that it has the ability to accommodate changes to the experimental protocol and make adjustments to the modeled spectra and concentration profiles without having to reconstruct the entire model.

The development of kinetic models may be beneficial to industry in a number of ways, all of which will help to eliminate the cost of mistakes, and may save the company time, materials, and money.

1.1 Formulation of Kinetic Models

It is clear that the development of kinetic models may be relevant to industry and useful for developing a complete understanding of a particular reaction system. The ease of construction of kinetic models greatly depends on the number of processes that have to be characterized in order to establish an accurate model and also depends on the complexity of the reaction at hand. The modeling of a simple first order reaction can be relatively simple, whereas modeling a more complex reaction with multiple steps and side products can be quite challenging. However, as long as the system follows elementary reaction principles, i.e. there is a one to one transfer of molecules from reactant to product, a kinetic model can be built. When supplemented with the use of spectroscopic measurements, concentration profiles for each component of a reaction mixture can be predicted along with the pure component spectra of the spectroscopically active components[6-9].

These models can be built using a variety of spectroscopic methods including ultraviolet/visible (UV/Vis), near infrared (NIR), and mid-infrared (Mid-IR)[10, 11]. The application of a kinetic model to a reaction system must be based on some form of measurement that can be directly related back to the concentrations of the reaction components. This is very true in the case of light absorption spectroscopy in that, generally, the

magnitude of an absorption signal is directly proportional to the concentration of a light absorbing species according to the Beer's-Lambert law.

The mathematical rate laws necessary for formulating the models are constructed from a set of reaction mechanisms known for the experiment in question. For instance, if it is known that a compound, "A", combines with another compound, "B", to form a product, "C", then the rate law equation can be easily constructed, as will be demonstrated later. These rate laws are excellent at predicting changes in concentration as a function of time, assuming that all initial concentrations and reaction rate constants are known. However, oftentimes during the development stages of the model, these values are not known and must be determined using measured spectroscopic data. Using Beer's law and a combination of the predicted concentration profiles made from the rate laws and the measured spectroscopic data from the experiment itself, the unknowns can be accurately predicted. When these unknowns are placed back into the rate law equations, they should be able to accurately predict the spectroscopic data. This process is termed "kinetic model fitting" and ensures that the mechanisms and rate law equations used in the model are appropriate for the system.

1.2 Modeling Reaction Processes

Kinetic model fitting can be used to describe many different chemical processes, not only reactions[12-19]. Any rate law that defines the changes in the concentration of a substance can be applied to a kinetic model. For example, rate laws can be written that have the ability to define changes in concentration due to dissolution and crystallization of materials within the system. When these crystallization and dissolution rate laws are assembled in

conjunction with the reaction rate laws, the changes in the concentration over time for a compound within the system can be accurately predicted. In this way, kinetic modeling is a very versatile technique that can be applied to almost any reaction system.

These models also have the ability to accurately distinguish between several spectroscopically active components and even predict the concentration profiles of reaction components that cannot be seen by a spectrometer within the active wavelength range. This is based on the changes in the spectra that correlate with the changes in the concentrations as a function of time. It is from this information that the model has the power to elucidate the pure component spectra for each of the spectroscopically active compounds in the reaction, regardless of spectroscopic visibility. The concentration profiles for all of the spectroscopically invisible components of the reaction can be indirectly determined based on the principle of mass balance when the reaction mechanisms are known precisely and are accurately represented by the rate law equations previously established.

In order to make these connections to the spectra, however, systems of ordinary differential equations must be used to specify the rates of change of each of these components as a function of time based on the estimated rate constants and the concentration of each component at any given moment. The predicted concentration profiles and the measured spectra are then used to calculate the pure component spectra for the data. The pure component spectra contain the absorption information for each of the spectroscopically visible species present in the reaction system. The pure component spectra along with the concentration profiles can then be used to calculate a set of estimated absorbance spectra in the reaction mixture as a function of time[7]. A residuals matrix is then calculated from the

difference of the measured spectra and the estimated spectra and can be used to evaluate the goodness of fit for the kinetic model.

The quality of the fit can be affected by numerous things including rate constants, initial concentrations, incorrect rate law functions, changes in volume, or other problems either in the building of the model or in the experimental protocol itself. To eliminate the effects of some of these problems, methods have been developed in order to optimize specific variables. For instance, it is unlikely that the reaction rate constants for all of the pieces of a particular reaction system are known exactly when trying to first establish a kinetic fit. The best way to determine the "true" value of these rate constants is to use a nonlinear optimization tool that evaluates the fit of the model after an initial guess of these values. The optimizer will then proceed through an iterative, systematic process to slightly alter the rate constant values that were initially specified until the goodness of fit is maximized[20, 21]. It is easy to recognize that performing all of these calculations would be impossible for a person to do quickly. To alleviate this, optimization tools are often built into high level data processing software, like MATLAB[22]. This makes the process of establishing a fit a much simpler process.

1.3 Challenges

Some reaction systems are more complex than others and present new challenges depending on the methods of measurement. Having the ability to detect all forms of the compounds that are present is not always possible, especially when working with an incompatible spectroscopic method. This incompatibility could be due to wavelength region, or the state of matter of the analyte being measured.

Certain methods of spectroscopy are limited in their ability to take measurements of specific media. For instance, Attenuated Total Reflectance (ATR) methods require the sample to be flush with the surface of an ATR crystal. An ATR measurement can only respond to light absorbing substances in a sample that are within a certain distance from its surface. The distance is dependent on the refractive index of the media surrounding the crystal and the operating wavelength of the spectrometer, as will be explained in more detail later. This short distance is indicative of the limitations in taking measurements of some samples, for example, solids suspended in solution. The size and shape of a solid particle does not allow the sample to be close enough to the crystal for a consistent measurement with a submersible probe in the UV/Vis range, as is used in this work[23, 24]. The opposite problem is present in a reflectance method of spectroscopy. Measurements taken using this technique are made using light that is emitted from a source that will hit a sample and then be reflected back to a detector[25]. However, the transmittance of light through a homogeneous liquid medium does not easily allow for the reflection and return of the emitted light to the detector. Because little light returns to the detector, the measurements made by the instrument may not provide enough information to make quantitative judgments. In many situations, diffuse reflectance based spectroscopic instruments are best suited to working with solid materials.

Recognizing these limitations is crucial when deciding what type of instrument to use when performing an experiment. In this work, one of the primary reaction mixtures being used is a slurry. A slurry is a mixture that contains a suspension of solid particles of a material in a liquid solvent. These types of mixtures are beneficial in industry because the product typically only needs to be dried before retrieval. The solvent used in the slurry may even be reused if no

reactions with the solvent took place. When performing a slurry reaction, a viable choice for spectroscopic measurements is NIR reflectance. When using a submersible fiber optic probe in a dense slurry, the suspended solid particles provide an excellent background for reflection. With a good source of reflection, both the liquid solvent and the solid particles present in the mixture have the ability to absorb the incident light with only confounding light loss due to scattering.

Despite being an acceptable system for reflectance measurements, it can be still difficult to monitor exactly what is going on in this kind of reaction mixture, which is why having a kinetic model is beneficial. In the slurry mixture used in this work, the solid particles suspended in the solvent are slightly soluble in that solvent. When the second reactant is pumped into the mixture, the dissolved portion of the solid reacts to form a product that is no longer soluble in the solvent, causing it to precipitate. This causes the equilibrium to shift, allowing more of the original solid reaction material to dissolve and react until the pumped in reactant has been totally consumed. In order to mathematically represent this reaction system, a model must be built for all of these processes. The dissolution of the solid reactant particles, the reaction of the dissolved particles with the second reactant, and the nucleation and crystallization of the product all must be modeled in order to accurately predict the concentration profiles of these components at any given moment during the experiment. It is for this reason that a simpler reaction model system was chosen in order to demonstrate the ability to model all of these phenomena separately before extending the kinetic model to the complex slurry system that incorporates all of them simultaneously.

1.4 Experiments of Interest

Initially, the goal of the work described here was to develop a kinetic model for an industrial slurry reaction developed by DuPont Crop Protection, of which the final product acts as an herbicide. The process used to make this product involves the dissolution of a solid form reactant, the reaction of that dissolved material with a second reactant that was pumped into the system, and the subsequent precipitation and crystallization of product. Up until this point, much work has been done to model these individual processes of reaction, dissolution, and crystallization separately. One of the goals of this work is to build a model that has the ability to characterize all of these processes together in one all-inclusive model.

The route used to develop the model for this system involved the use of a well-known and well understood model system that incorporated all of the same processes as the slurry reaction. The synthesis of acetylsalicylic acid (aspirin) has been extensively studied[11, 14, 26, 27] and provides all of the necessary elements for the modeling of this system. The initial addition of solid salicylic acid dissolves in a solvent, acetic anhydride, and then proceeds to react to form the product, acetylsalicylic acid. Once the product has formed, it will precipitate. These processes are shared by the slurry reaction, with only difference being that the slurry reaction has all of these phenomena taking place simultaneously, whereas the synthesis of aspirin has a separate crystallization step. Despite this difference, the aspirin synthesis model provides an excellent example for the capabilities of kinetic modeling.

2. Theory

Developing a kinetic model requires the full understanding of a number of processes. This includes having knowledge of the spectroscopic techniques used to measure the reaction mixture, the formation of reaction mechanisms and rate laws, the creation of ordinary differential equations, the numerical integration method used to integrate these differential equations, and the optimization algorithm used in the model fitting. Together, these processes make up the groundwork of kinetic model fitting.

2.1 Spectroscopic Methods

2.1.1 ATR UV/Vis

Attenuated Total Reflectance (ATR) Ultraviolet-Visible (UV/Vis) spectroscopy is the first of the two spectroscopic methods used in this work. UV/Vis spectroscopy operates in the 180-700 nm wavelength range, and is a commonly used tool in industrial and research measurements[28]. When combined with an ATR probe, it has the unique ability of only taking a measurement of a very thin layer of the sample in direct contact with the ATR probe[24]. A submersible three bounce ATR UV/Vis is illustrated in Figure 1. The light emitted from the source reflects off each surface of the crystal before returning to the detector.

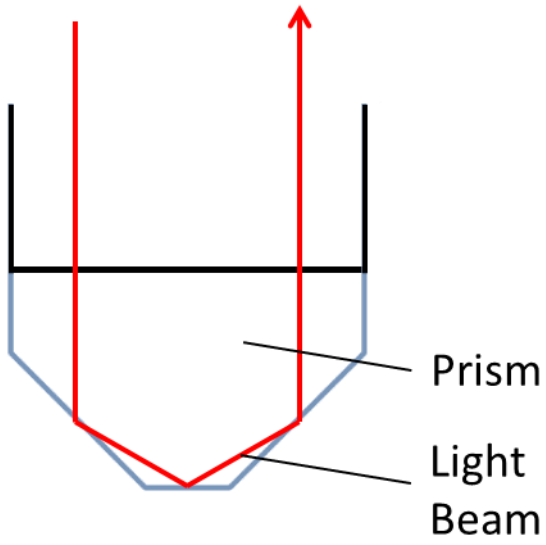

Figure 1. Diagram of a three bounce ATR UV/Vis probe.

Each surface of the crystal is designed to utilize the concept of Total Internal Reflection, where the incident light from the source strikes the crystal surface at an angle such that complete internal reflection is achieved (Figure 2). When the incident light strikes a surface at an angle that is greater than the "critical angle", the light will completely reflect off of the surface, with none escaping into the surrounding medium. If the angle of incidence were smaller than the critical angle, the light would pass through the boundary surface and into the media. These probes are specifically designed so that at each surface of the crystal, the angle of incidence of the light beam is greater than the critical angle.

ATR sample measurements utilize an evanescent field that crosses over the boundary created by the crystal surface and dips into the surrounding media, as shown in Figure 2.

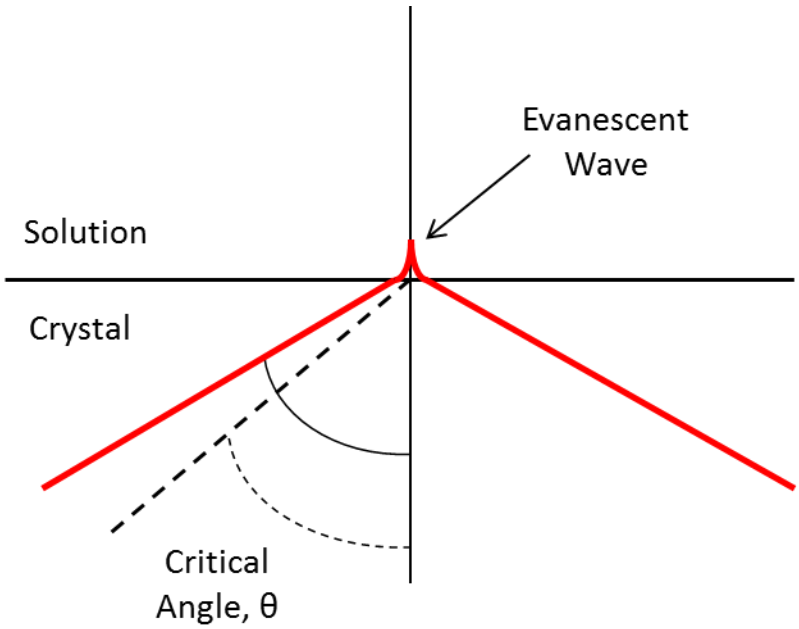

Figure 2. When the beam strikes the crystal surface at an angle greater than the critical angle, the beam is reflected. When the beam is reflected it also forms an evanescent field that reaches into the surrounding media where some wavelengths may be absorbed.

When this evanescent field crosses over the crystal surface, the media immediately surrounding the crystal has the ability to absorb the light intensity in the same way as any transmission spectroscopic technique. In UV/Vis spectroscopy, specific wavelengths of light have the ability to excite electrons within atomic orbitals or molecular orbitals to different energy levels. Different orbitals exhibit characteristic energy levels that result in the excitation of electrons at different wavelengths as light is absorbed, thus resulting in the spectral variances seen in different molecules.

One of the unique things about ATR measurements in the UV/Vis wavelength range is that the evanescent field does not extend far past the surface of the crystal. The depth of penetration of this field is dependent on both the wavelength of light, the refractive index of the surrounding media, and the refractive index of the crystal. In the Near Infrared and Mid-

Infrared wavelength ranges, the evanescent field can extend into the sampling media about 2,500 nm to 30,000 nm, respectively. However, in the UV/Vis range, the field can only reach about 70 nm into the surrounding media. When working within this small range, it becomes almost impossible to measure any solid form that is present in the surrounding media[24]. This technique is used primarily to determine the contents of a solution phase in direct conatact with the probe. Concentrations of solid phase materials in the sample cannot be measured explicitly, but can be indirectly calculated. Using a system of rate laws and differential equations, the concentrations of the spectroscopically active species in the solution can be used to indirectly calculate the concentrations of the non-active species, such as the solid particles using the principle of mass balance. This will be explained in more detail later.

2.1.2 NIR Reflectance

The Near Infrared spectroscopic region (NIR) refers to the wavelength range between 700 and 2500 nm. NIR spectroscopy is becoming a more commonly used technique in industry for many reasons. Not only is the instrumentation relatively affordable, but it is easy to use and maintain, and little to no sample pretreatment is necessary if using the correct tools. Alongside modern data processing techniques, NIR spectroscopy can be as powerful a tool as Mid-IR and UV/Vis spectroscopy[29].

In this work, NIR spectroscopic measurements are made in a diffuse reflectance sampling mode. This sampling method measures the intensity of light that reflects off of the surface of a sample. Unlike ATR UV/Vis, this technique is best suited for taking measurements of solid samples. Although NIR wavelengths have the ability to be absorbed by liquid samples, no reflected light can be returned to the detector when no reflective surface is present. A solid

sample provides an excellent backdrop for these kinds of measurements, as the solid particles provide a surface for the light to reflect off of. This is shown in more detail in Figure 3.

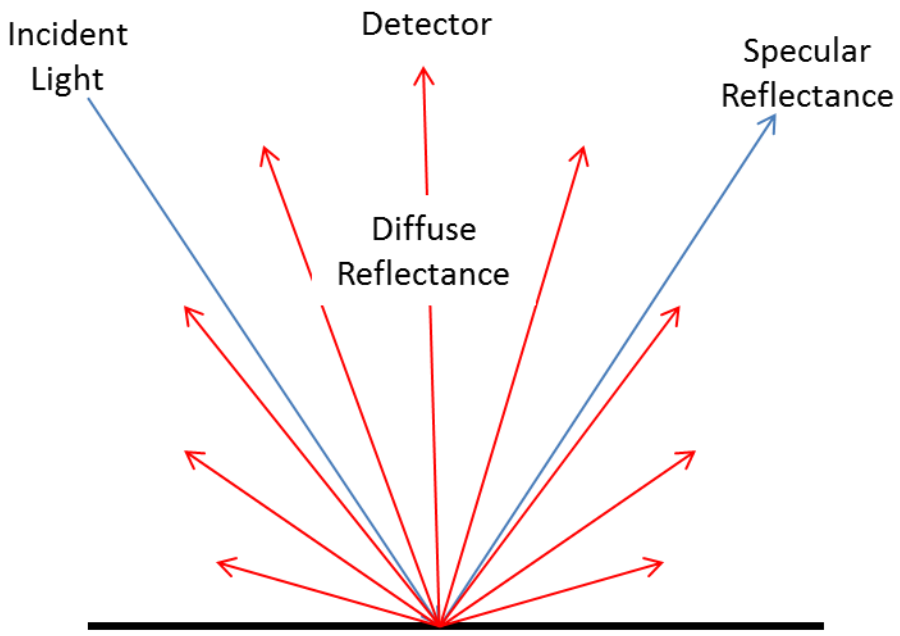

Figure 3. Diffuse reflectance spectroscopy. A beam of light is shined onto a solid sample. This beam then scatters off of the surface of the sample and returns to the detector.

Reflectance measurements, however, do have limitations when working with solid media. When the incident light strikes the surface of the sample, the varying angles of the light waves entering and exiting individual solid particles can result in the scattering of light off of the sample surface in multiple directions. This scattering of light can result in the loss of signal, giving an inaccurate reading. Some scattered light will return to the detector, but oftentimes the light scatters away from the probe and is not measured. If extensive, the loss of signal due to scattering can result in the inability to accurately characterize the sample being measured, making light scattering one of the largest challenges involved with NIR diffuse reflectance measurements. Use of an integrating sphere in the sample chamber can be used to capture

light scattered in all directions; however, such a sampling device is not suited for online measurements with fiber optic probes.

Regardless of this fact, diffuse reflectance methods remain some of the best for taking measurements of solid particles and are also ideal for working in dense slurry mixtures. Since a dense suspension of solid particles in a slurry is present in the experiments studied in this thesis, it can provide an excellent backdrop for reflectance measurements.

2.2 Kinetic Modeling

2.2.1 Beers-Lambert Law

In order to relate the absorption measurements to the actual concentrations of the solution being sampled, the Beers-Lambert law is used[28].

$$y = \varepsilon c l \tag{2-1}$$

In this form of the equation, y is the spectroscopic absorbance, ε is the molar absorptivity of the solute ($L \cdot mol^{-1} \cdot cm^{-1}$), c is the concentration of the solute ($mol \cdot L^{-1}$), and l represents the pathlength (cm). This equation is also applicable to mixtures of multiple chemical species, and can be represented as a linear combination of the concentrations, absorptivites, and pathlengths for n species as shown in Equation 2-2. Because the pathlength for all species will remain the same, the absorptivity, ε, and pathlength, l, are combined into a single term, a.

$$y = c_1 a_1 + c_2 a_2 + \ldots + c_n a_n \quad (2\text{-}2)$$

The values of *c* and *a* can also be represented across multiple wavelengths and times and can be replaced in the equation above with vectors representing the concentration for each species as a function of time and each absorptivity as a function of wavelength. Because this equation can be represented as a linear combination of multiple species, the equation can be represented in matrix form.

$$\mathbf{Y} = \mathbf{CA} + \mathbf{R} \quad (2\text{-}3)$$

The symbol, **Y**, represents the *m* × *n* absorbance matrix for the data set, **C** is an *m* × *k* matrix containing the concentrations of *k* species present in the mixture across *m* intervals of time, also known as the concentration profile, and **A** is a *k* × *n* matrix containing the pure component spectra across *n* wavelengths for each of the species[7]. In kinetic modeling, when the modeled **C** and **A** terms are multiplied they create an estimated form of the matrix **Y** designated as $\mathbf{Y}_{calc}$. The difference between these matrices **Y** and $\mathbf{Y}_{calc}$ produces a matrix of residuals, **R**. The residual matrix is later used to establish the goodness of fit for the kinetic model. A visual form of this equation is shown in Figure 4.

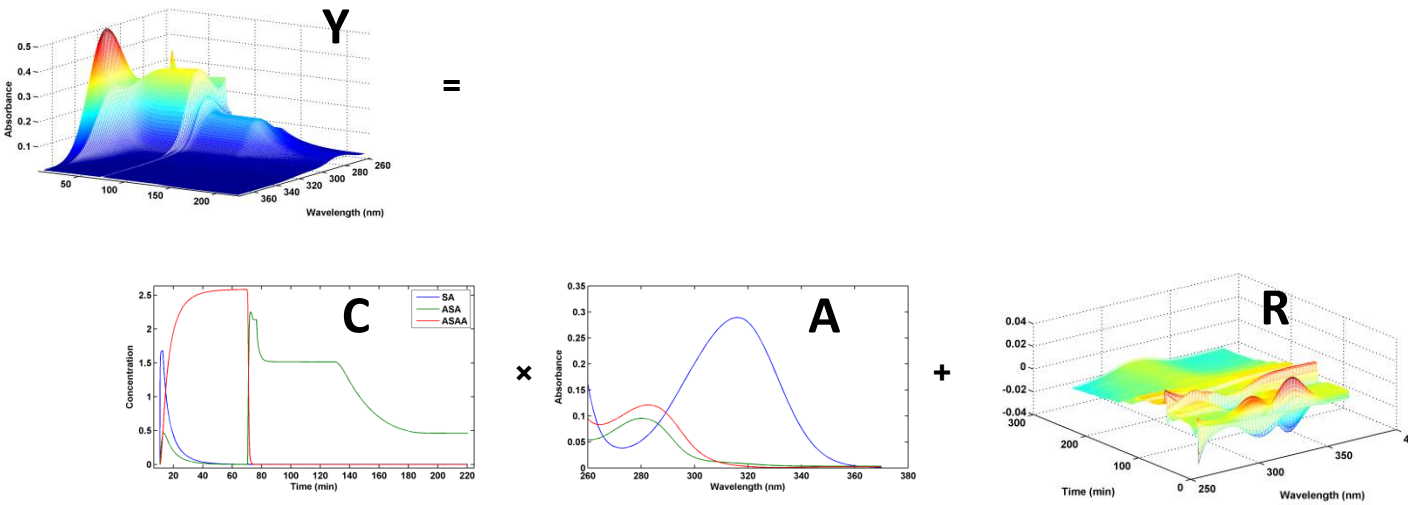

Figure 4. Illustration of the Beers-Lambert law. The term **Y** is the spectroscopic data as a function of time and wavelength, **C** contains the concentration profiles of the spectroscopically active species, and **A** contains the pure component spectra for each of the spectroscopically active species. The term **R** is the matrix of residuals based on the difference of the measured and estimated spectra.

2.2.2 Rate Laws and Ordinary Differential Equations

In order to fit a kinetic model to a matrix of time-dependent spectroscopic measurements, the first thing that must be done is to build concentration profiles depicting the changes over time of the concentrations of all the components in the reaction mixture[6]. The concentration profiles themselves are constructed from a system of ordinary differential equations (ODEs) that define the rate of change for the concentration of each species as a function of time. To make these ODEs, the rate laws for each chemical process must first be defined. Knowledge of each of these processes is necessary for building an accurate kinetic model that yields an estimated set of spectra that matches the spectra that are measured experimentally.

In order to determine the rate law equations and ODEs necessary for determination of the concentration for any species at any given moment, the components and reaction mechanisms must be known. For example, in a simple second order reaction system, a reaction

mechanism can be written displaying all of the reactants and products for a particular reaction along with the reaction rate constant.

$$2\mathrm{A} \xrightarrow{k_{2\mathrm{A}}} \mathrm{B} \tag{2-4}$$

The mechanism shows that two equivalents of a species A react to form a product B. This mechanism is then used to define the rate law for this particular reaction.

$$r = k_{2\mathrm{A}}[\mathrm{A}]^2 \tag{2-5}$$

From the rate law, the ODEs for each of the reaction components can be established.

$$\frac{\mathrm{d}[\mathrm{A}]}{\mathrm{d}t} = -2k_{2\mathrm{A}}[\mathrm{A}]^2 = -2r \tag{2-6}$$

$$\frac{\mathrm{d}[\mathrm{B}]}{\mathrm{d}t} = k_{2\mathrm{A}}[\mathrm{A}]^2 = r \tag{2-7}$$

These differential equations are then integrated as function of time in order to calculate the concentrations for A and B at any moment in time, *t*.

$$[\mathrm{A}] = \frac{[\mathrm{A}]_0}{1 + 2[\mathrm{A}]_0 k_{2\mathrm{A}} t} \tag{2-8}$$

$$[\mathrm{B}] = [\mathrm{B}]_0 \frac{[\mathrm{A}]_0 - [\mathrm{A}]}{2} \tag{2-9}$$

2.2.3 Numerical Integration

Unfortunately, for many multi-step reactions, it is impossible to directly integrate the ODEs and compute the concentrations for each of the reaction species using standard formulaic approaches, due to the higher order of the reaction and multiple steps. In order to integrate the ODEs, a numerical integration method must be used.

Numerical integration methods have the ability to compute a close approximation of the concentration as it changes over time based on a technique initially described by Euler's method. This is done by taking a single concentration of a species at a time, t, and calculating the rate of change of the concentration from the ODEs and then estimating the concentration at a new time, t_n, where:

$$t_n = t_{n-1} + n\Delta t \tag{2-10}$$

The accuracy of this estimation depends greatly on the step size, Δt, used to move through the data, and the rate of change in the concentration at that moment. If the curvature of the function is great, then a smaller step size is necessary to capture the changes in the curve. For instance, if the rate of change is great while the step size is large, then the shape of the concentration curve will not be accurately captured, and a great deal of descriptive information will be lost, leading to inaccuracies in the concentration profiles. However, if the rate of change is great and the step size is small, then the shape of the curve will be estimated with a greater deal of accuracy, providing a concentration profile that is faithful to the actual experimental changes in concentration. Euler's method is illustrated visually in Figure 5.

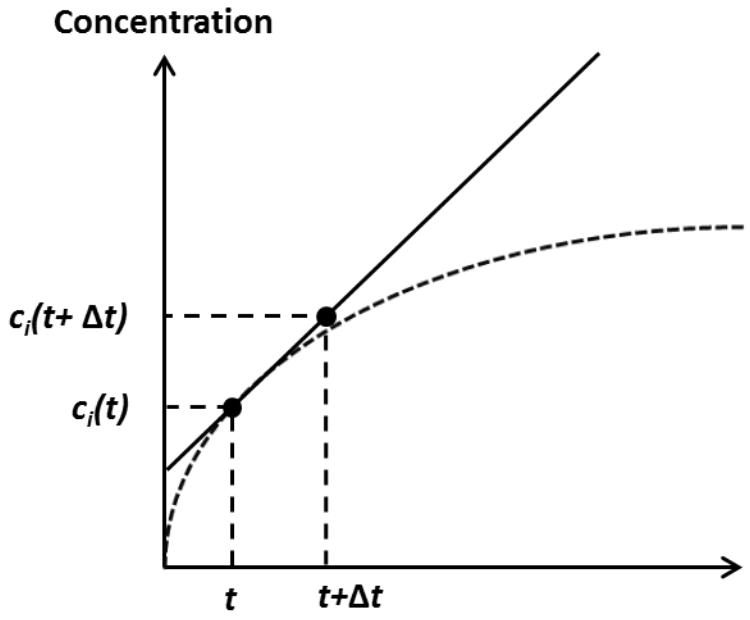

Fig. 5. Euler's method. The rate of change in the concentration at time, t, is calculated and then is used to estimate the concentration at time, $t + \Delta t$.

Euler's method serves as an excellent example as to how numerical integration processes work, but is not able to make accurate predictions for more complex problems. A numerical integration method that is more commonly used is the classical Runge-Kutta method. The classical Runge-Kutta method works in much the same way as Euler's method[30]. The primary difference is that it is a fourth order integration method, meaning that instead of using two data points of distance Δt to establish an extrapolation of the curve, it uses five. The use of five data points along this fitted curve enables use of a fourth order polynomial for extrapolation, which gives a much more accurate estimate of the value of the concentration from step to step, providing a concentration profile that has a greater ability to accurately represent the data. There are other forms of the Runge-Kutta method that utilize a quadratic polynomial fit to three points to define the curve, however the fourth order version provides

greater precision and is more commonly used. Fortunately, the numerical integration techniques are often built into high level data processing software, like MATLAB[22], so it has become much easier to integrate systems of ODEs in an automated fashion.

2.2.4 Nonlinear Optimization

When formulating a kinetic model fitting algorithm, some necessary values may be unknown. For example, the rate constants for the reactions are typically unknown for different reaction systems. If the rate constants used are incorrect, the model will produce concentration profiles that do not accurately portray the data. This will, in turn, produce an estimated set of spectra that does not accurately complement the original experimental data.

In order to alleviate this problem, techniques are available to optimize experimental parameters that may not be exactly known at the beginning of the model fitting process. One such optimization method is the Newton-Gauss-Levenberg-Marquardt (NGLM) algorithm[20, 21]. This method uses the set of residuals, **R**, calculated in Equation 2-3 as a basis for comparison when optimizing adjustable parameters. The algorithm adjusts the initial value of the parameters iteratively, using the new value to recalculate a set of estimated spectra from the rate law equations and ODEs. As the estimated spectra get closer to the actual measured values, the values in **R** will get smaller. The sum of squares of the residual matrix, *ssq*, decreases with the values in **R**, and is used to gauge the fit of the model.

First, all of the parameters being optimized, such as the reaction rate constants, must have an initial guess value. After these values are selected, the guessed parameters are used in the first integration of the ODEs used to describe the rate laws. Once this is done, concentration

profiles are constructed and then used to calculate an estimated set of spectra via the numerical integration method discussed in the previous section. The residual matrix is then calculated and then used to determine the *ssq* value that represents the fit of the model.

$$ssq = \sum_{i=1}^{nt}\sum_{j=1}^{n\lambda} r_{i,j}^2 \tag{2-11}$$

Ideally, the *ssq* value should be as close to the error attributed to the measurement as possible. For example, if the measurement error of a system is 0.01 absorbance units, then an ideal value of *ssq* should be as close to 0.01 as possible, assuming the measurement errors are normally distributed and uncorrelated.

Initially, a vector **p** contains all of the initial guess values for the parameters that are being optimized by the algorithm. The decrease in the values of **R** is due to small changes that are made to these parameters. These changes to **p** are contained within the shift vector, Δ**p**. Unfortunately, it is not inherently obvious how changes to each element of **p** will affect **R**. Utilization of the Taylor series expansion, however, can provide guidance as to the value and magnitude of the elements in Δ**p**. A crude approximation for the new matrix **R** can be calculated by summing the previous value with the derivative of **R** with respect to each parameter as shown in Equation 2-12.

$$\mathbf{R}(\mathbf{p_0} + \Delta\mathbf{p}) \approx \mathbf{R}(\mathbf{p_0}) + \frac{\partial \mathbf{R}(\mathbf{p_0})}{\partial p_1}\Delta p_1 + \frac{\partial \mathbf{R}(\mathbf{p_0})}{\partial p_2}\Delta p_2 + \cdots + \frac{\partial \mathbf{R}(\mathbf{p_0})}{\partial p_{np}}\Delta p_{np} \tag{2-12}$$

The resulting equation is linear, and in an ideal situation the primary interest is in finding the exact quantities contained in the vector Δ**p** that will create a perfect match between the

estimated and measured spectra. If an exact solution is found, then in the absence of experimental error, the ideal value of $\mathbf{R}(\mathbf{p}_0+\mathbf{\Delta p})$ is zero. Assuming $\Delta\mathbf{p}$ will give this result, the term $\mathbf{R}(\mathbf{p}_0+\mathbf{\Delta p})$ can be set to zero and the equation can be rearranged.

$$\mathbf{R}(\mathbf{p_0}) \approx -\frac{\partial \mathbf{R}(\mathbf{p_0})}{\partial p_1}\Delta p_1 - \frac{\partial \mathbf{R}(\mathbf{p_0})}{\partial p_2}\Delta p_2 - \cdots - \frac{\partial \mathbf{R}(\mathbf{p_0})}{\partial p_{np}}\Delta p_{np} \tag{2-13}$$

In realistic situations, when the value of **p** is close to the actual solution, the values of $\mathbf{R}(\mathbf{p}_0+\mathbf{\Delta p})$ will be small enough that successive approximate estimates of $\mathbf{\Delta p}$ will converge to the actual solution. The method of finite differences can be used to estimate the partial derivative of **R** with respect to each parameter in **p**. This technique uses a shift Δp_i to adjust an individual element *i* of **p** to calculate **ΔR**, where the change will be due only to the parameter being adjusted. The difference between the new value of **R** and the old is taken and divided by the shift value, thus giving an approximation of the change in **R** as a function of the parameter p_i, shown in Equation 2-14.

$$\frac{\partial \mathbf{R}(\mathbf{p_0})}{\partial p_i} \approx \frac{\mathbf{R}(\mathbf{p_0} + \Delta p_i) - \mathbf{R}(\mathbf{p_0})}{\Delta p_i} \tag{2-14}$$

In the limit as $\mathbf{\Delta p}$ approaches zero, the approximation in Equation 2-14 becomes very good. The magnitude of the shift, Δp_i, must be chosen to be as small as possible without incurring substantial round-off errors inherent in floating point calculations carried out on a computer. The output of the finite difference method is individual matrices, each detailing the change in the elements of the residual matrix as a function of the individual parameters, p_i. The matrices

attributed to each parameter are then assembled into a three dimensional matrix. A data cube such as this is computationally demanding for a computer and is not ideal to work with.

To solve this problem, the new matrices containing the partial derivative information for the residuals are vectorised. Each column of the matrix is stacked one on top of the other in order to create a single vector. The new vectors associated with the partial derivatives for each adjustable parameter are then arranged side by side into a matrix called the Jacobian matrix, **J**, where each column vector of the matrix contains the numerical estimate of the derivative for each parameter.

$$\mathbf{r}(\mathbf{p_0}) = -\mathbf{J}\Delta\mathbf{p} \tag{2-15}$$

The information is now in a form that can be solved in a least squares manner.

$$\Delta\mathbf{p} = -\mathbf{J}^{+}\mathbf{r}(\mathbf{p_0}) \tag{2-16}$$

These shift vectors are added to the original values of the parameters in **p**, and replace the previous values. These new parameters are then used to reintegrate the ODEs and build new concentration profiles. The new concentration profiles are then used to calculate a new set of estimated spectra that are in turn used to calculate a new value of *ssq* that is lower than the previous value.

This process is repeated iteratively until *ssq* reaches the desired level of convergence. As the residuals in **R** get smaller, the value of *ssq* will decrease as well, and as the adjusted parameters get closer to their optimum values, *ssq* will change less with each iteration. Once the magnitude of the difference between the new and old *ssq* values fall below a certain

threshold, the *ssq* can be assumed to remain constant and the algorithm will end. When the algorithm ends, the outputs are the new values of the parameters, optimized to provide the best possible fit for the measured data using the equations provided by the model.

Unfortunately, problems can arise when the initial estimates are poor. In some cases, the value of *ssq* begins to diverge due to innaccuracies in the initial approximations of the parameters during the Taylor expansion. These poor estimates may lead to incorrect derivations in the change in **R** with respect to the parameters, producing residuals that are worse than before. To deal with this problem, Marquardt proposed the addition of a new term called the Marquardt parameter, *mp*. When the NGLM algorithm mentioned previously reaches a point where the *ssq* value begins to increase instead of decrease, an *mp* term is added to the diagonal of what is known as the Hessian matrix. The Hessian matrix is equal to the product of the Jacobian matrix and its transpose, which is represented within the pseudo-inverse of the Jacobian shown in Equation 2-16. Since, the Hessian matrix has a direct effect on the size of the shift vector, multiplying the Hessian by the scalar value *mp* has the ability to significantly increase or decrease the value of $\Delta\mathbf{p}$. If the value of the parameter was not at the optimum value, then this change should result in a decrease in the residuals. The size of *mp* is iteratively increased by a factor of ten as long as the value of *ssq* remains larger than the last value prior to its divergence. Once *ssq* decreases past the previous value at which *ssq* diverged, *mp* is iteratively decreased at set intervals until it reaches a value of zero. Once *mp* is set to zero again, the algorithm continues to adjust parameters in the same manner as before. The NGLM process is visually represented by a flow chart in Figure 6.

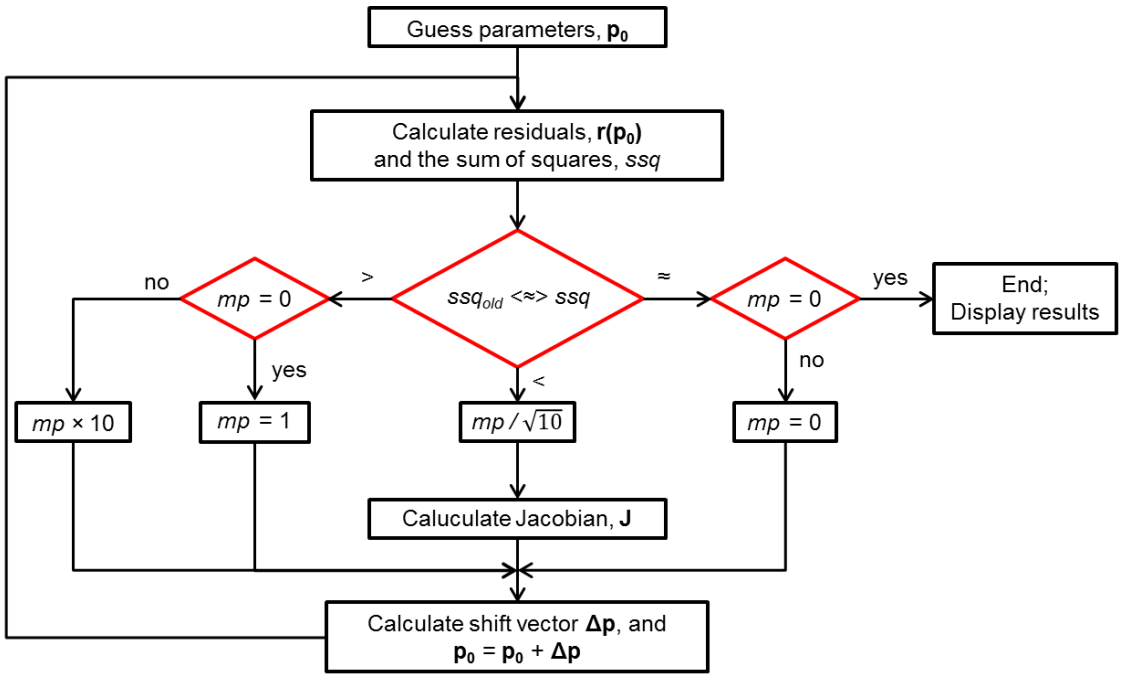

Figure 6. Newton-Gauss-Levenberg-Marquardt (NGLM) algorithm. The algorithm ends when difference in *ssq* and ssq_{old} passes a specified threshold. It is very unlikely the two will ever be exactly equal.

2.2.5 Complete Kinetic Model

For the sake of understanding the modeling process, an example will be presented here to assist in tying these processes together. Knowledge of the reaction mechanism is necessary for building an accurate kinetic model. If the stoichiometry of the reaction is incorrect or all of the components are not considered, then the rates described by the ODEs may not be able to fully describe the spectra. Consider the following reaction mechanism for a two-step reaction:

$$\mathrm{A} + \mathrm{B} \xrightarrow{k_1} \mathrm{C} \tag{2-17}$$

$$2\mathrm{C} \xrightarrow{k_2} \mathrm{D} \tag{2-18}$$

From these mechanisms, two rate law equations can be established, one for each reaction process that takes place in the system.

$$r_1 = k_1[\mathrm{A}][\mathrm{B}] \tag{2-19}$$

$$r_2 = k_2[\mathrm{C}]^2 \tag{2-20}$$

Now that the rate laws have been established, the ODEs can be specified for each of the components present in the reaction system. These ODEs describe the rates of change in the concentration of each component as a function of time.

$$\frac{d[\mathrm{A}]}{dt} = \frac{d[\mathrm{B}]}{dt} = -r_1 \tag{2-21}$$

$$\frac{d[\mathrm{C}]}{dt} = r_1 - 2r_2 \tag{2-22}$$

$$\frac{d[\mathrm{D}]}{dt} = r_2 \tag{2-23}$$

The rate terms, r_n, are either positive or negative depending on whether that component is being produced or consumed, respectively. For instance, the species C is a product in the first reaction and, therefore, the rate of formation is described as a positive value, r_1. However, C is a reactant in the second reaction and is therefore described by a negative rate of consumption, $-r_2$. The sum of the contributions from the rate laws describe the total change in the concentration of the species C as a function of time, as shown in the ODEs in Equations 2-21 through 2-23.

At this point, the reaction rate equations needed for the kinetic model are present. In order to use these equations, certain values must be ascertained. Initial concentrations for each of the reaction components and the reaction rate constants are necessary to construct the concentration profiles. The reaction rate constants are very likely unknown values, and must be optimized through the kinetic model fitting. In order for the the model fitting process to begin, initial guesses for these rate constants must be made.

Using these initial values for the concentration and rate constants, the concentration profiles can be constructed defining the concentrations of each species as a function of time. Using these concentration profiles and the measured set of spectra, the pure component spectra for each of the observable components can be calculated through the restatement and rearrangement of the Beers-Lambert Law.

$$\mathbf{Y} = \mathbf{CA} \Rightarrow \mathbf{A} = \mathbf{C}^{+}\mathbf{Y} \tag{2-24}$$

When the product of the matrices **C**, containing the concentration profiles, and **A**, containing the pure component spectra is calculated, it creates the matrix of estimated spectra, $\mathbf{Y}_{calc}$. The difference between the matrix containing the measured spectra, **Y**, and the matrix of estimated spectra is used to then calculate the matrix of residuals, **R**.

$$\mathbf{R} = \mathbf{Y} - \mathbf{CA} = \mathbf{Y} - \mathbf{Y}_{calc} \tag{2-25}$$

From here, the sum of squares of the residuals is calculated, and is used to establish how well the model fits the data. Using the residual matrix **R** and the value of *ssq*, changes are made iteratively to the nonlinear parameters using Equations 2-12 through 2-16, calculating a

shift vector that decreases the residuals and, in turn, *ssq*. As the residuals get smaller, *ssq* will begin to converge. Once the difference between the newly calculated *ssq* and the previous one has passed a certain threshold, the algorithm ends. At the end of the NGLM algorithm, these newly optimized parameters are used to calculate a set of estimated spectra that accurately mimic the measured spectra.

3. Kinetic Modeling of Dissolution, Reaction, and Crystallization Processes in the Synthesis of Acetylsalicylic Acid

Abstract:

Kinetic modeling of batch reactions has been shown to be a helpful method for developing a complete understanding of a reaction system along with providing a useful method for on-line batch process monitoring. Much work has been done to demonstrate the ability to model dissolution, reaction and crystallization processes separately, however little has been done in terms of combining all of these into an all-inclusive kinetic model system. The goal of this work is to demonstrate the integration of dissolution and crystallization processes into a kinetic model to accurately predict concentration profiles and spectroscopic measurements in slurries. The model system selected for this work was an acetylsalicylic acid synthesis reaction, a relatively well known and well understood reaction. Presented here is a successful kinetic model for the dissolution of salicylic acid, the reaction of salicylic acid with acetic anhydride to form acetylsalicylic acid, and the subsequent crystallization of the product where crystallization was driven by a cooling process and the model incorporated solubility as a function of temperature.

3.1. Introduction

The development of kinetic models for use in modeling and monitoring of batch reaction processes has been an active area of research in the last decade [1, 27, 31]. Modeling

of reaction systems is helpful for acquiring a complete understanding of a production process and has demonstrated its usefulness in providing new methods with which to monitor large scale batch reactions[32]. Monitoring of reactions in this manner has both safety and financial benefits. For instance, if a mistake is caught due to an error that was found due to the system's inability to fit within the acceptable limits of the model, corrections may be able to be made in order to save the batch and prevent a waste of materials and time.

Much work has been done in order to model reactions and reaction processes. Modeling of reactions, dissolutions, and crystallization processes have been a frequent area of study [12, 15, 17, 33] , and each has become a well understood process. However, usefulness in a practical setting is limited due to the fact that little work has been done to combine these methods into one cohesive model. Although modeling each of these processes separately provides a great deal of information, a model that incorporates each of them simultaneously would provide information for the complete model system all at once.

Presented here is a method for characterizing the dissolution, reaction, and subsequent crystallization of an acetylsalicylic acid synthesis, all within a single kinetic model system.

3.2. Theory

Under certain limiting assumptions (described later), kinetic models have the ability to accurately predict absorbance and concentration profiles for all components of a reaction system as a function of time. In order to do this, a mathematical model should be fit to a set of

measured spectra for the system. An excellent tutorial is provided by Puxty [6] for the process of fitting kinetic models, so only a summary will be provided here.

3.2.1 Beer-Lambert Law

The calculations used to determine the predicted absorbance at a given moment are based on a simple restatement of the Beer-Lambert law as a linear combination of the terms across multiple times and wavelengths for a number of species present in the reaction mixture:

$$\mathbf{Y} = \mathbf{CA} + \mathbf{R} \tag{3-1}$$

where **Y** is an $m \times n$ matrix containing the measured spectra as a function of time and wavelength, **C** is an $m \times k$ matrix containing the concentration profiles across m times for each of some number, k, of absorbing species present in the system, **A** is a $k \times n$ matrix containing the absorptivity profiles of each species as a function of n wavelengths, and **R** is the $m \times n$ matrix of residuals which represent random measurement error. In the most common form of Beers law, there are separate terms for molar absorptivity and pathlength[28], however, in this case, both terms are combined into the term A, due to the relative consistency of the pathlength.

The product of the matrices **C** and **A** provide the estimate for the mixture spectra in the process as they evolve over time which are used to fit the model system. In order to establish how well the model fits the measured spectra, the sum of the squares of the residual matrix is calculated.

$$ssq = \sum r_{ij}^{\ 2} \tag{3-2}$$

3.2.2 Constructing Concentration Profiles

The construction of accurate concentration profiles is the foundation for an accurate kinetic model system. The concentration profiles are produced by numerical integration of a system of ordinary differential equations (ODEs) to calculate the changes in concentration for each species present in the system as a function of time. In order to do this, there must be an understanding of the reaction mechanisms that take place in the system. For example, consider a simple second order reaction:

$$2\mathrm{A} \xrightarrow{k_{2\mathrm{A}}} \mathrm{B} \tag{3-3}$$

where k_{2A} is the reaction rate constant. Using this mechanism, a set of ODEs can be constructed.

$$\frac{\mathrm{d}[\mathrm{A}]}{\mathrm{d}t} = -2k_{2\mathrm{A}}[\mathrm{A}]^2 \tag{3-4}$$

$$\frac{\mathrm{d}[\mathrm{B}]}{\mathrm{d}t} = k_{2\mathrm{A}}[\mathrm{A}]^2 \tag{3-5}$$

For such a simple system, the ODEs can easily be integrated to calculate the concentration at any given moment in time. However, for most multi-step reaction systems it becomes impossible to integrate the ODEs directly, so a numerical integration process must be used.

The classical Runge-Kutta method [34] of numerical integration is used in this work. This method has proven to be faster and more accurate than other numerical integration techniques including Euler's method and the second order version of the Runge-Kutta technique.

These numerical integration techniques are frequently built into high level data processing software packages, but still require the system of ODEs to be constructed beforehand. The actual method for ODE construction is based on the rate law equations determined from the reaction mechanisms. For instance, in the two step reaction:

$$\mathrm{A} + \mathrm{B} \xrightarrow{k_1} \mathrm{C} \tag{3-6}$$

$$2\mathrm{C} \xrightarrow{k_2} \mathrm{D} \tag{3-7}$$

a rate law equation can be made for each of the two reactions.

$$r_1 = k_1[\mathrm{A}][\mathrm{B}] \tag{3-8}$$

$$r_2 = k_2[\mathrm{C}]^2 \tag{3-9}$$

The differential equations that are associated with each species present in the reaction can then be derived. The sign of the rates calculated in Equations 3-8 and 3-9 are dependent on

whether the material in question is consumed or produced, and the sum of these values can be used to directly calculate the total rate of change for each material.

$$\frac{d[\mathrm{A}]}{dt} = \frac{d[\mathrm{B}]}{dt} = -r_1 \tag{3-10}$$

$$\frac{d[\mathrm{C}]}{dt} = r_1 - 2r_2 \tag{3-11}$$

$$\frac{d[\mathrm{D}]}{dt} = r_2 \tag{3-12}$$

Using these differential equations and a numerical integration method, it is straightforward to calculate the concentration profiles for each of the components of the reaction mixture. The remaining information that is required is the initial concentrations of each species present and the reaction rate constants for each reaction. In this work the initial concentrations are known, but the rate constants are not known. In order to determine these values, a nonlinear optimization routine is used.

3.2.3 Newton-Gauss-Levenberg-Marquardt Algorithm

The Newton Gauss Levenberg Marquardt (NGLM) algorithm [20, 21] is used here to optimize unknown parameters, specifically the reaction rate constants. These constants will vary with different experimental conditions because they are influenced by external conditions,

such as temperature. An optimization technique such as NGLM is useful for finding accurate estimations of these parameters that best describe the measured data.

In order to calculate the concentration profiles, there must first be a set of initial guesses for all of the parameters that are to be optimized. Using this first estimate of the concentration profiles, a set of estimated spectra are calculated.

$$\mathbf{Y} = \mathbf{CA} \Rightarrow \mathbf{A} = \mathbf{C}^{+}\mathbf{Y} \tag{3-13}$$

The difference in the estimated and measured spectra create the matrix of residuals that are then used to calculate *ssq*. The optimization algorithm proceeds iteratively, calculating shifts in the initial parameters resulting in a decrease in the residuals and, in turn, a decrease in *ssq*. The first term in a truncated Taylor series expansion [6, 30] is used to calculate a shift in each of the nonlinear parameters that will decrease the residuals, coinciding with a set of estimated spectra that better represent the original measured spectra with each iteration of the algorithm. The adjusted parameters are then used to calculate a new set of concentration profiles. This process of minimizing residuals by calculating shift vectors continues until *ssq* converges to a minimum value and the process ends. Eventually, the residuals will approach their minimum value, and *ssq* will change very little across iterations of the algorithm. When the difference between the newly calculated *ssq* and the old *ssq*, passes a certain threshold, the algorithm ends. In this work, the convergence was complete when the difference was less than 1×10^{-4}.

3.3. Experimental

The model system chosen for this work was an acetylsalicylic acid synthesis reaction, including the dissolution of the solid reactant salicylic acid (SA), the reaction of SA in the solution with acetic anhydride (AA) to form the products acetylsalicylic acid (ASA) and acetic acid (HA), and the subsequent crystallization of the product. This reaction was chosen due to the fact that it is a well-known and well-understood reaction. It was also ideal for the modeling in this work in that dissolution, reaction, and crystallization processes occur under appropriate conditions within one relatively short experimental period.

3.3.1 Equipment

All experiments were run in a custom 50 mL computer controlled reactor system made in-house at East Carolina University including a heated oil jacket. Heated silicone oil was pumped through the jacket and a 20 W hastalloy auxiliary heating coil with a proportional-integral-derivative (PID) controller was used to maintain specified temperatures inside the reactor vessel. All of these were controlled using an HEL Inc. automate™ system operating under the HEL WinISO software package. The reactor lid contained openings for a UV/Vis submersible attenuated total reflectance (ATR) probe, the PID heating coil, a hastalloy temperature probe connected to the temperature control software, and tubing connected to an automatic syringe pump used to inject liquid reagents into the system. The syringe pump was also controlled by the WinIso software.

All UV/Vis measurements were taken using a tec5USA multi-channel spectrophotometer (Plainview, NY) with a resolution of 3 nm in the 190-1100 nm regions, using a fiber-optic submersible Hellma probe with a three-bounce sapphire ATR crystal. Data was collected using the MultiSpec Pro software designed by tec5USA.

Validation of the kinetic modeling results was performed using an off-line HPLC system. The measurements were performed using an Agilent Zorbax Eclipse C-18 (25 cm x 4.6 mm, 5 µm) column at 40°C, with an injection volume of 15 µL and a flow rate of 1 mL/min. The mobile phase was a 60:40 water (adjusted with 1% v/v acetic acid) and methanol mixture.

3.3.2 Method

A 20 mL aliquot of AA (Fisher Scientific) and a 0.2 mL aliquot of phosphoric acid catalyst (Fisher Scientific) was added to the reactor and then heated to 55° C. The oil jacket was maintained at 55° C by a Julabo heater/chiller. Approximately 9.5 g of SA (Fisher Scientific) was then added to the solution and allowed to undergo dissolution. During this period both dissolution and reaction took place simultaneously. Due to the abundance of AA present in the solution, the product ASA underwent a second reaction to form the side product acetylsalicylic anhydride (ASAA) [35-37]. After 60 minutes, an addition of 4 mL of water was delivered by the computer controlled syringe pump at a rate of 1 mL/min to destroy the anhydrous side product and the remaining AA. The side product reacted with water to reform the product ASA along with HA. At this point, the solution was supersaturated with ASA and unseeded nucleation and crystallization occurred stochastically. Once the solution reached equilibrium, the reactor was cooled at a rate of -1.5°C/min until the reactor reached 5°C. The computer controlled system

maintained a constant temperature drop of -1.5° C between the jacket and reaction mixture during the linear cooling ramp. This cooling section of the experiment was added in order to demonstrate the robustness of the model across varying temperatures and to demonstrate the ability to include temperature induced crystallization into the comprehensive kinetic model. An example for the spectra taken in this experiment is provided in Figures 7 and 8.

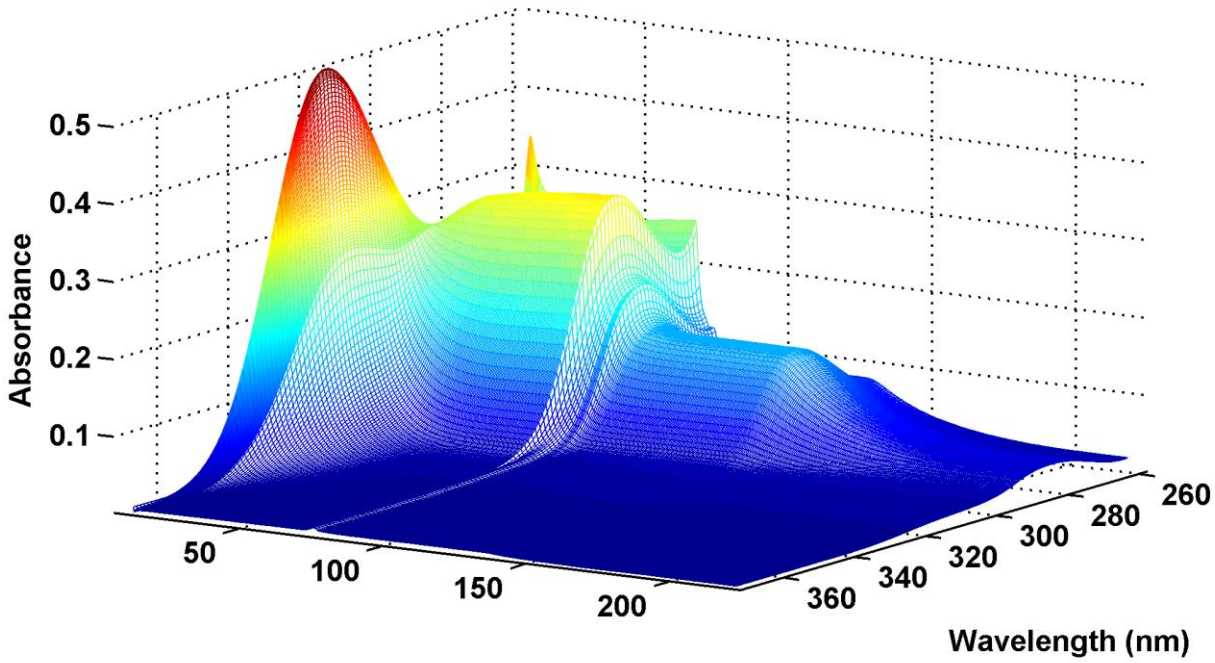

Figure 7. ATR UV/Vis absorbance as a function of time and wavelength.

3.3.3 Reaction Rate Laws

As mentioned previously, building a kinetic model starts with establishing a set of ODEs used to construct the concentration profiles for each of the species in the reaction. In order to do this with accuracy, the reaction mechanisms must be known and a set of rate law equations must be established. Four reaction mechanisms were considered in the kinetic model for this

experiment. In the first step of the experiment, SA was added to the solution. As ASA formed, it proceeded to react a second time with AA to form the side product ASAA.

$$\mathrm{SA} + \mathrm{AA} \xrightarrow{k_1} \mathrm{ASA} + \mathrm{HA} \tag{3-14}$$

$$\mathrm{ASA} + \mathrm{AA} \xrightarrow{k_2} \mathrm{ASAA} + \mathrm{HA} \tag{3-15}$$

After the addition of water, the system undergoes another set of reactions which convert the side product to ASA and consume the excess AA.

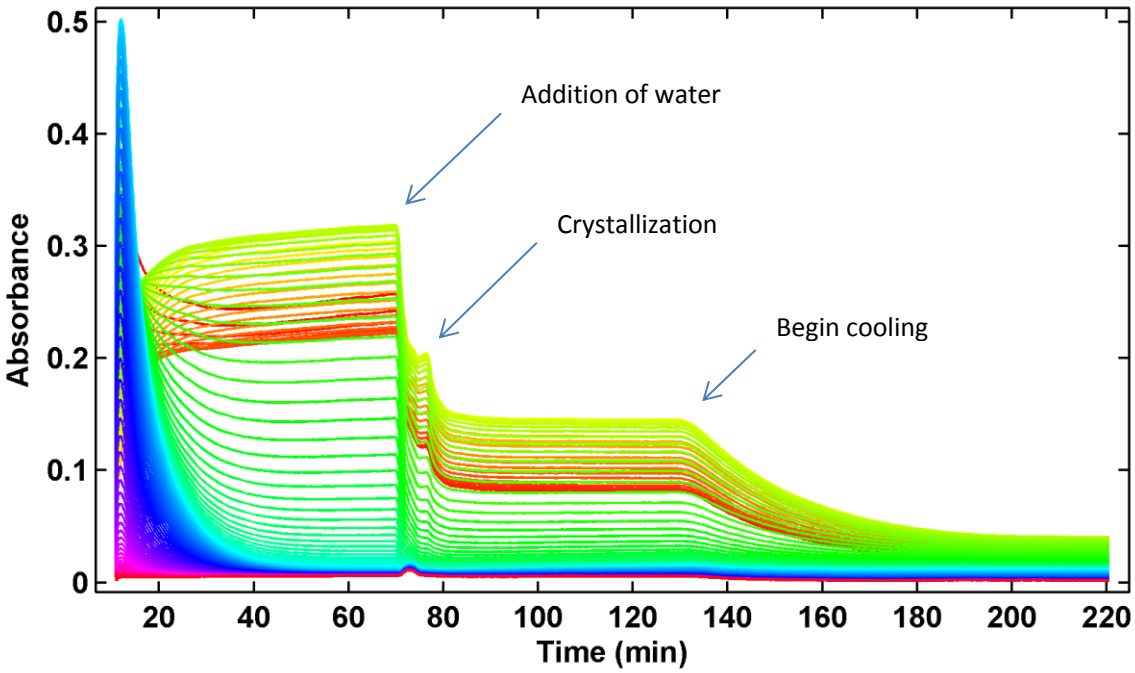

Figure 8. ATR UV/Vis spectra of the ASA reaction from 260 to 370 nm shown plotted as a function of time. Spectra begin with the addition of solid SA to the reactor. The SA simultaneously dissolves and reacts to form ASA which then reacts again to form side product, ASAA. At approximately 70 minutes water is pumped into the reactor, resulting in a large drop in absorbance due to the destruction of ASAA. At approximately 77 minutes crystallization occurs, resulting in a second drop in absorbance. At 130 minutes, cooling begins.

$$\mathrm{ASAA} + \mathrm{H_2O} \xrightarrow{k_3} \mathrm{ASA} + \mathrm{HA} \tag{3-16}$$

$$\mathrm{AA} + \mathrm{H_2O} \xrightarrow{k_4} 2\mathrm{HA} \tag{3-17}$$

The mechanisms are then converted into a series of rate law equations for use in determining the ODEs.

$$r_1 = k_1[\mathrm{SA}][\mathrm{AA}] \tag{3-18}$$

$$r_2 = k_2[\mathrm{ASA}][\mathrm{AA}] \tag{3-19}$$

$$r_3 = k_3[\mathrm{ASAA}][\mathrm{H_2O}] \tag{3-20}$$

$$r_4 = k_4[\mathrm{AA}][\mathrm{H_2O}] \tag{3-21}$$

In order to construct a comprehensive model, rate law equations for the dissolution and crystallization processes must also be included.

3.3.4 Dissolution and Crystallization Rate Laws

Modeling dissolution and crystal growth rate processes are slightly different than modeling reactions. Detailed models have been developed to provide accurate descriptions for the rates of dissolution and crystallization.

3.3.4.1 Crystal Growth

The rate of crystal growth[14, 38], r_g, can be described by Equation 3-22.

$$r_g = \frac{\Phi_s M_s k_c}{3 d_s \Phi_v} \eta_r (C - C_{sat})^g \tag{3-22}$$

The terms Φ_s and Φ_v are the surface and volumetric shape factors, respectively, for the solid particles, M_s is the molecular weight of the solid, d_s is the density of the solid, η_r is the effectiveness factor[39], and k_c is the crystallization rate constant. The term C is representative of the instantaneous concentration of the solute and the term C_{sat} is the concentration of the solute in a saturated solution.

In our work, we assumed that most of these variables do not undergo an appreciable change during the course of the experiment, so the rate laws can be condensed into a simpler form[40].

$$r_c = k'_c (C - C_{sat})^c \tag{3-23}$$

The term r_c represents the crystallization rate. In crystallization, the driving force is determined by the degree of supersaturation.

Replacing the terms C and C_{sat} with the concentrations of ASA in the synthesis reaction, the appropriate rate law equations are created that can be used for the construction of the ODEs specific to this batch process.

$$r_c = k'_c ([\mathrm{ASA}] - [\mathrm{ASA}]_{sat})^c \quad (3\text{-}24)$$

3.3.4.2 Dissolution

The rate of dissolution[41, 42], r_d, is very similar to the rate of crystal growth shown in Equation 3-22.

$$r_d = \frac{2M_s k_d}{d_s}(C_{sat} - C) \quad (3\text{-}25)$$

The term k_d is the dissolution rate constant. Unlike the rate of crystal growth, the rate of dissolution is dependent on the degree of undersaturation. Similarly, this rate law can be simplified.

$$r_d = k'_d (C_{sat} - C)^d \quad (3\text{-}26)$$

When the terms C and C_{sat} are replaced with the concentrations of SA, the appropriate rate law equation for the construction of the ODEs is formed.

$$r_d = k'_d ([\mathrm{SA}]_{sat} - [\mathrm{SA}])^d \quad (3\text{-}27)$$

3.3.5 Building the ODEs

From these rate law equations, the system of ODEs can be established for each component of the reaction system.

$$\frac{d[\mathrm{SA}]_{\mathrm{solid}}}{dt} = -r_d$$

$$\frac{d[\mathrm{SA}]}{dt} = r_d - r_1 - \frac{dV}{dt}\frac{[\mathrm{SA}]}{V}$$

$$\frac{d[\mathrm{AA}]}{dt} = -r_1 - r_2 - r_4 - \frac{dV}{dt}\frac{[\mathrm{AA}]}{V}$$

$$\frac{d[\mathrm{HA}]}{dt} = r_1 + r_2 + r_3 + r_4 - \frac{dV}{dt}\frac{[\mathrm{HA}]}{V}$$

$$\frac{d[\mathrm{ASAA}]}{dt} = r_2 - \frac{dV}{dt}\frac{[\mathrm{ASAA}]}{V}$$

$$\frac{d[\mathrm{ASA}]}{dt} = r_1 - r_2 + r_3 - r_c - \frac{dV}{dt}\frac{[\mathrm{ASA}]}{V}$$

$$\frac{d[\mathrm{H_2O}]}{dt} = -r_3 - r_4 + f\frac{[\mathrm{H_2O}]_{in}}{V} - \frac{dV}{dt}\frac{[\mathrm{H_2O}]}{V}$$

$$\frac{d[\mathrm{ASA}]_{\mathrm{solid}}}{dt} = r_c$$

Each of the *r* terms are representative of the rates previously established by the rate laws shown in Equations 3-18 through 3-21. The sign of *r* indicates whether the species is being consumed or produced in that reaction step. The term *f* is the flow rate of water into the system, and *V* is the total volume of solution.

The term *dV/dt* represents the change in volume as a function of time. We assumed volumes were additive in this model and include terms to account for volume changes due to the addition of water, dissolution of solid SA, crystallization of ASA, and changes in the partial molar volume of each reactant and product. As the reaction proceeds and water is added to the system, the total volume of the solution increases, causing a dilution of each of the components, in turn, resulting in a decrease in the concentration. The total change in volume was calculated based on the partial molar volumes for each component[43]. The total volume of the solution is the sum of the partial molar volumes in the solution:

$$V_{tot} = n_1 v_1 + n_2 v_2 + \cdots + n_n v_n \tag{3-28}$$

where *n* is the number of moles of a species, and *v* is the partial molar volume of that species in mL/mol. When *n* is replaced by a vector $\mathbf{r}_i$ containing the rates of change of the concentration for a species *i*, the change in volume as a function of time can be calculated:

$$\frac{dV_i}{dt} = v_i V(\sum r_{i,j}) \tag{3-29}$$

where *V* is the total volume of solution in mL. As an example, the change in total volume attributed to SA includes dissolution, r_d (a net volume increase), and its consumption, r_1 (a net volume decrease).

$$\frac{dV_{SA}}{dt} = v_{\mathrm{SA}}[V(r_d - r_1)] \tag{3-30}$$

When the sum of these is taken for all species, as demonstrated in equation 3-31, the rate of change of the total solution volume can be calculated.

$$\frac{dV}{dt} = \frac{dV_{\mathrm{SA}}}{dt} + \frac{dV_{\mathrm{AA}}}{dt} + \frac{dV_{\mathrm{ASA}}}{dt} + \frac{dV_{\mathrm{HA}}}{dt} + \frac{dV_{\mathrm{ASAA}}}{dt} + \frac{dV_{\mathrm{H_2O}}}{dt} \tag{3-31}$$

3.3.6 Temperature Calibration

A calibration experiment was performed to determine the temperature dependent solubility curve for ASA in order to properly model ASA's rate of crystallization. The calibration experiment was conducted in-situ using a reaction slurry mixture at various temperature intervals. This test was an extension of the experiment detailed in Section 3.3.2.

After cooling a reaction mixture to 5°C (278 K), the temperature was raised in seven intervals of 5°C to a final temperature of 50°C (323 K). The well-stirred slurry containing precipitated ASA was allowed to reach equilibrium for 10 minutes at the end of each heating step. The establishment of equilibrium was verified by observing a constant UV/Vis absorbance at the ASA absorption maximum of 283 nm. At each interval, the concentration of ASA in the solution phase was calculated mathematically using the measured UV/Vis ATR spectra and its pure component spectrum. Changes in the ATR absorbance of the pure component spectra over the temperature range of 5° C to 50° C was less than 2% and deemed negligible for the purpose of constructing the ASA solubility curve. The resulting calibration curve and equation is shown in Figure 9.

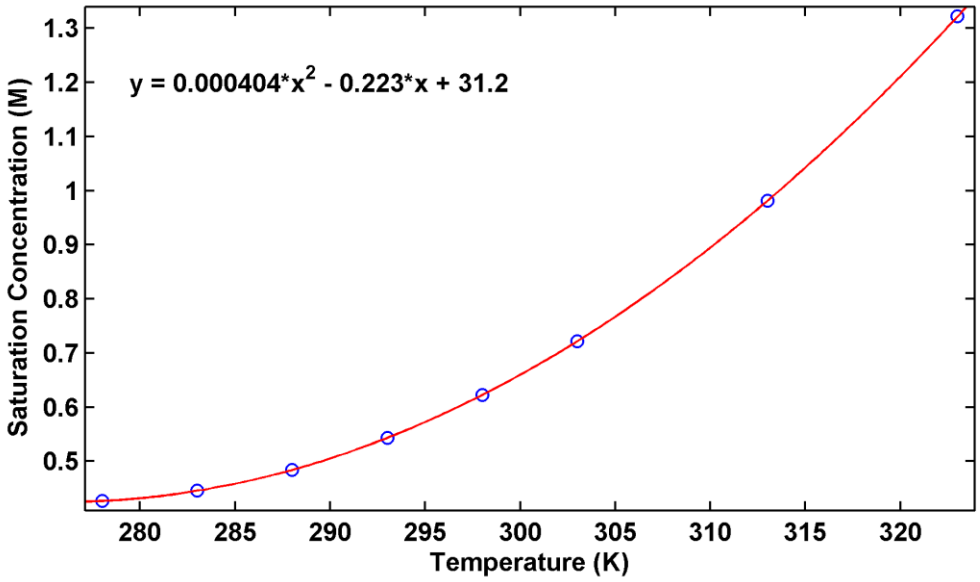

Figure 7. ASA quadratic solubility curve from 5° C to 50° C.

3.4. Results

Using the ODEs and the NGLM non-linear optimization method, concentration profiles were constructed for all spectroscopically active species present in the reaction mixture. In these experiments the set of spectroscopically active species included SA, ASA, and the side product, ASAA as shown in Figure 10. Only the spectroscopically active species in this wavelength range can be modeled directly from the data using this method. Attempting to directly model more than these will result in a rank deficient matrix inverse during the model fitting process[44]. In this experiment, the rank of the pure component concentration matrix, **C**, and pure component spectral matrix, **A**, (see Equation 3-1) is three due to the fact that the mixture spectra directly change in relation to three compounds, i.e. the compounds active in the UV/Vis range. From this information, the concentration profiles of the remaining

spectroscopically inactive species (AA, HA, H_2O) can be indirectly calculated from the principles of mass balance, resulting in the concentration profile shown in Figure 11.

Using the set of spectroscopically active concentration profiles, an estimate of the process absorbance spectra can be directly computed. A side-by-side comparison of a set of measured and estimated UV/Vis spectra can be seen in Figure 12.

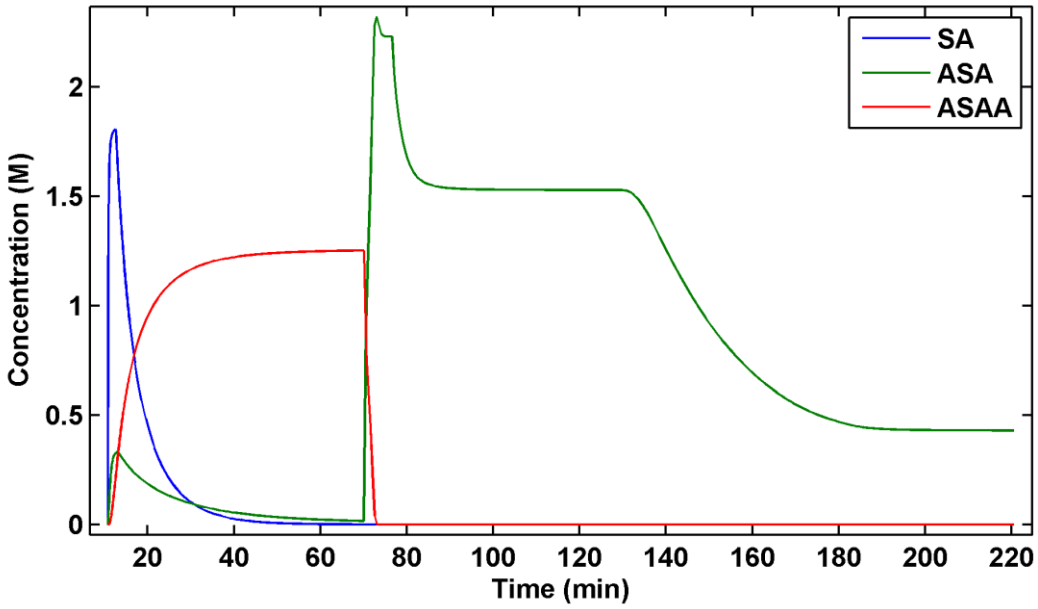

Figure 8. Concentration profiles for the spectroscopically active species constructed by the ODEs and optimized by the NGLM method.

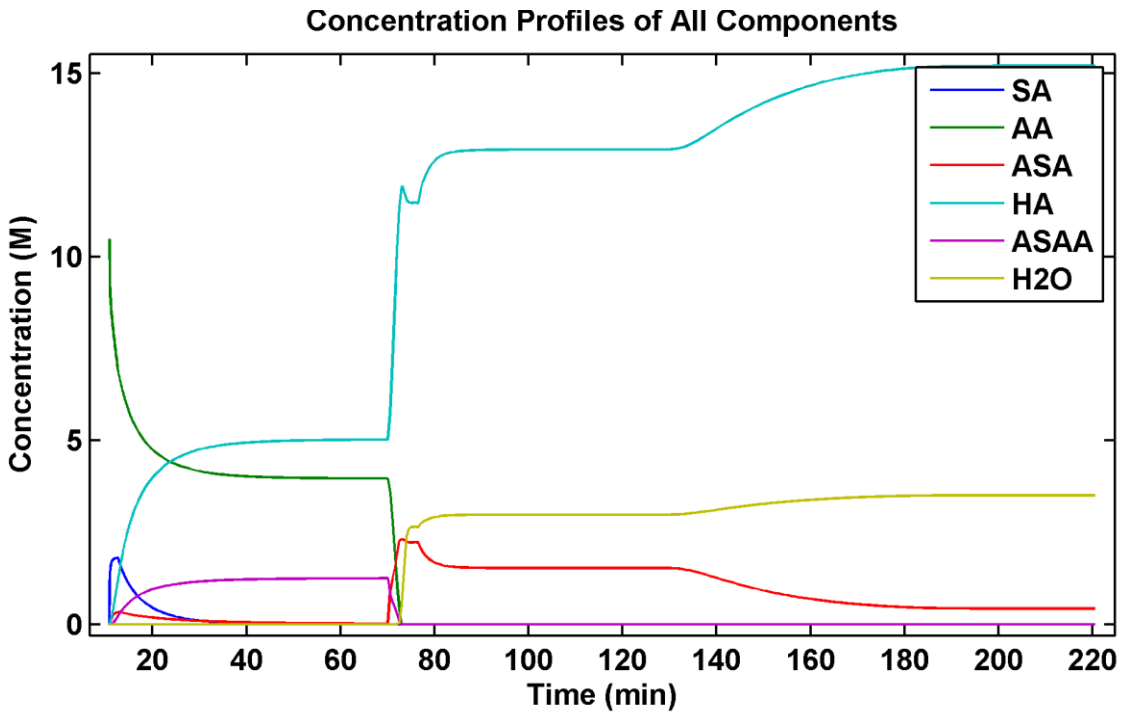

Figure 9. Concentration profiles for all species present in the reaction mixture. Solid SA is added at the onset of the experiment, reacting immediately with the AA that is present, resulting in the formation of product and side product. At approximately 70 minutes, water is added to the system, eliminating the side product and consuming the excess AA. At approximately 78 minutes, the crystallization event occurs, followed by a decrease in temperature at 130 minutes.

The concentration profiles of each species follow a predictable trend as SA dissolves and is consumed to form the products and side products. During the addition of water at 70 minutes, the side product and remaining AA is rapidly consumed to form ASA and HA. A small peak can be observed in the concentration profiles of HA and ASA at approximately 75 minutes prior to the onset of precipitation. At the time when the reactants AA and ASAA have been completely consumed, water is still being added to the reaction mixture by the syringe pump. This results in a dilution effect as the total volume of the solution mixture continues to increase while the number of moles of each species

remains constant. The decrease in concentration stops when the pump is turned off at approximately 76 minutes.

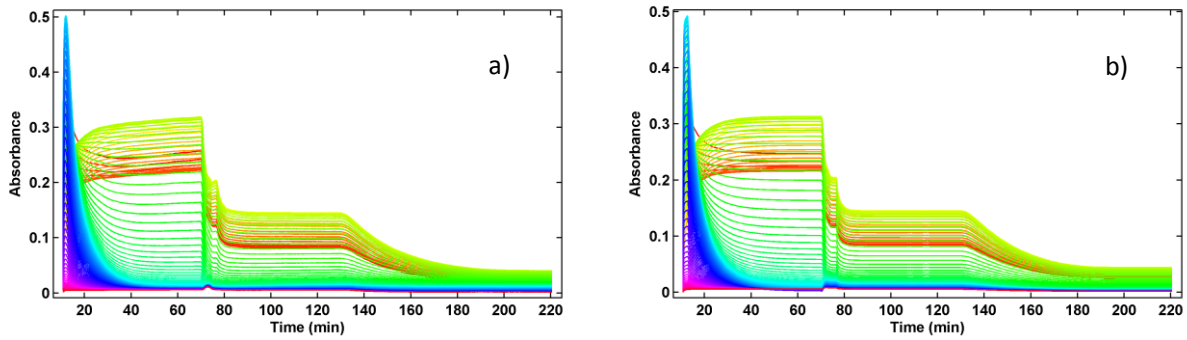

Figure 10. Figure 12a shows the absorption profiles from the measured spectra and 12b shows the estimated absorption profiles predicted by the model.

The modeled spectra show good agreement with the measured spectra, with an *ssq* value of 0.9541. However there are some apparent visual discrepancies between the two figures. In particular, in Figure 12a there is a small but noticeable drift (increase) in absorbance between 30 and 70 minutes and again on the plateau between 75 and 77 minutes. It is believed that this phenomenon is due the weak adsorption of analyte on the surface of the ATR crystal, because it only takes place during periods of supersaturation. This type of phenomenon was regularly observed in this work, and has been reported by others using UV/Vis ATR sampling methods similar to the one used here under supersaturated conditions [33].

A better visual representation of the model fit is shown in Figure 13. The spectral profile isolated was at 283 nm, the location of the peak maximum for the spectral band of the product and near the maximum of the side product. The circles in the figure represent the measured spectra while the line represents the modeled spectra. The estimated spectra give a very close

approximation to the measured spectra, with the primary deviations being attributed to the supersaturation adsorption phenomena mentioned previously.

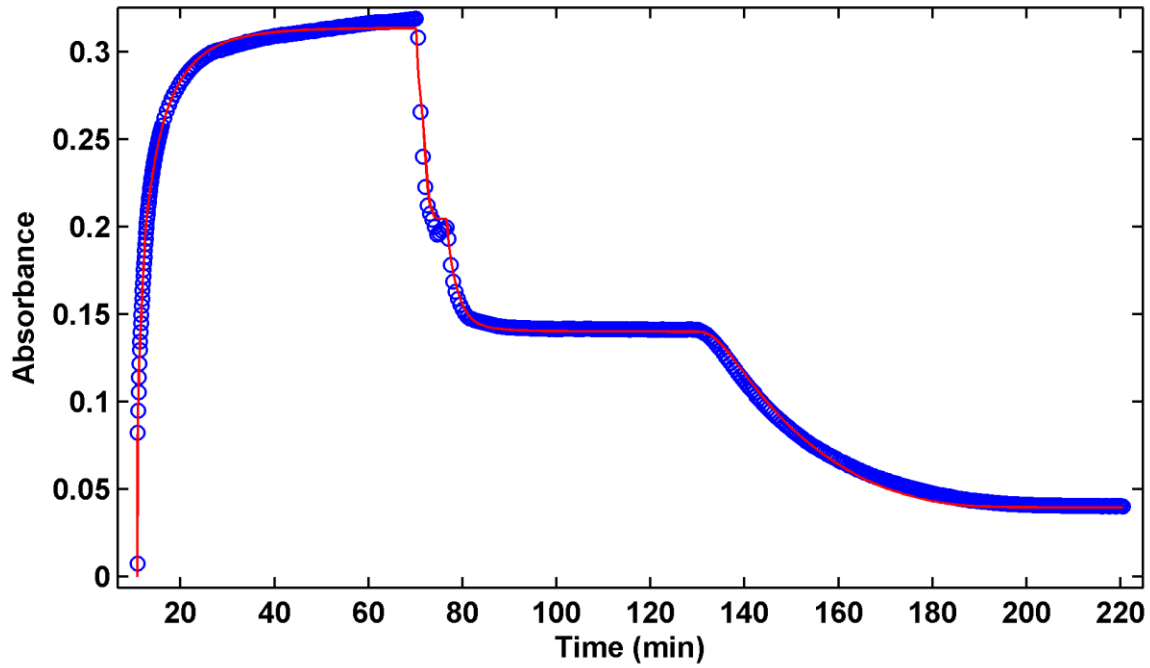

Figure 11. Measured (cirlces) and estimated (line) spectral profiles for the reaction at 283 nm: the location of the peak maximum for ASA and the side product.

The results from the non-linear optimization are shown in Table 1. The unknown values in this work consisted primarily of reaction rate constants. The value k_1 is the constant for the reaction of SA with AA to form the product, k_2 is for the reaction of the product to form side product, k_{w1} is the constant for the reaction of the excess AA with water, k_{w2} is the constant for the reaction of the side product with water to re-form the product, k_d is the dissolution rate constant for SA in the solution, and k_c is the crystallization rate constant for ASA. The saturation concentration of SA in the reaction mixture was also unknown and could not be readily calculated since the experiments were performed in a neat solution and would dissolve and react immediately; so, this value was also optimized.

Table 1. Optimized values for two experiments using the NGLM non-linear optimization method. The *ssq* values that were used to establish the goodness of fit are also shown.

	Exp. 1	**Exp.2**
k_1	0.03385	0.03395
k_2	0.2636	0.4191
k_d	7.081	7.128
k_{w1}	1.025E+03	8.480E+02
k_{w2}	79.68	83.60
k_d	1.112	1.014
$[SA]_{csat}$	2.067	2.067
ssq	0.9541	0.9476

Two replicate batches were conducted for the comparison shown in Table 1. One was performed on June 23, 2011 and the other on July 7, 2011. The results shown in Table 1 demonstrate the relative consistency in the model fitting. There are some noticeable differences between estimated parameters for the two data sets, however. In particular, the differences between the values of k_{w1} are especially significant, but these differences are likely due to the fact that the exothermic reaction of AA with water occurs rapidly over a timespan where only a few spectra are taken. It is therefore, very challenging to get an accurate estimate of this value. There is also a significant discrepancy between the values of k_2, attributed to the reaction rate of the formation of side product, ASAA. We can speculate that this difference was due to experimental error during the manual addition of SA to the reaction vessel, but the reason for this discrepancy remains unknown. The purpose of this model fitting procedure was to develop an empirical model that demonstrates an accurate depiction of how the concentration of reactive species change over time, producing a companion set of estimated

pure component spectra and mixture spectra that are statistically similar to the experimentally measured spectra.

The similarities between the two batches can be seen in Figure 14. This figure displays an overlay of the results similar to those shown in Figure 13 for the two data sets referred to in Table 1. The shapes of the spectral profiles are very similar in most places, but in the locations where there are differences, the modeled spectra agree with the measured spectra that they correspond to. This demonstrates the robustness of both the model and the system itself. The differences between the two data sets are due to the slight differences in the initial concentrations of the individual reaction mixtures.

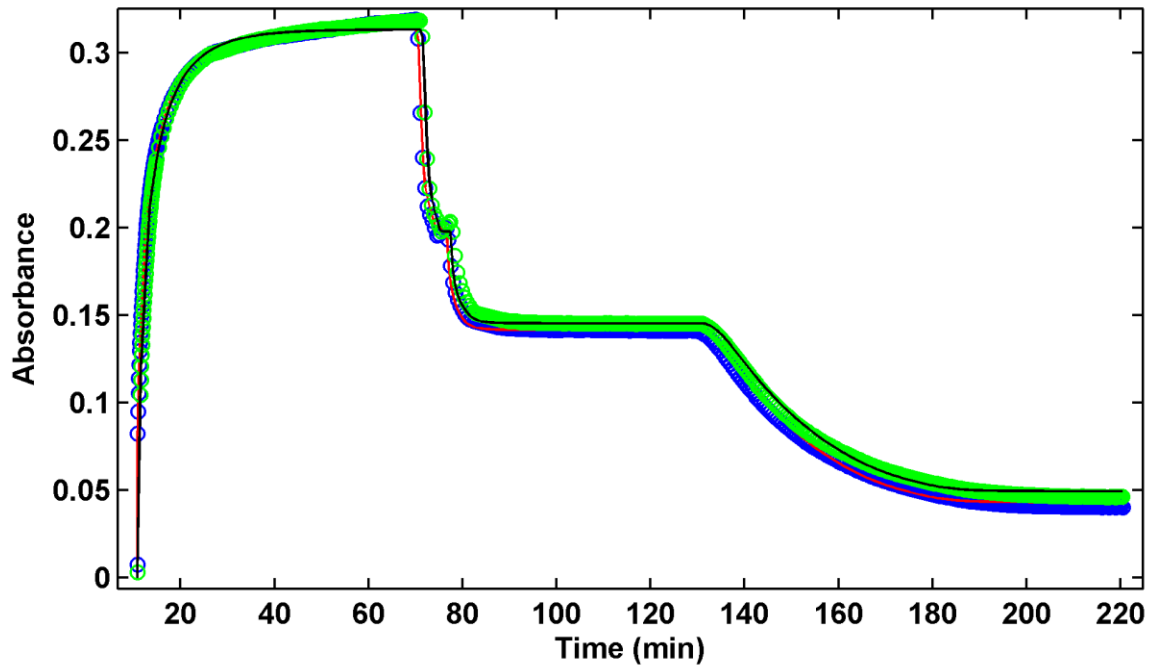

Figure 12. Spectral profiles of two data sets at 283 nm. The blue circles and red line indicate the measured and estimated spectra, respectively, for one data set while the green circles and black line are the measured and estimated spectra for the second data set.

In order to confirm the findings, a validation of the concentration profiles was performed via HPLC measurements. Adjustments were made to the initial experimental protocol mentioned in section 3.3.2 in order to facilitate sample-taking. Only the cooling portion of the protocol was altered. In the validation work, the temperature was dropped by increments of 10°C instead of being lowered at a constant rate. After allowing for equilibration of the well stirred system at each temperature level, the stirrer was momentarily turned off, and the solid particles were allowed to settle to the bottom of the reactor. Because the ATR sampling method only has the ability to detect the solution immediately surrounding the crystal, only the solution phase of the mixture was withdrawn for validation by HPLC. Three 50 µL replicate samples were taken at 55 °C before crystallization occurred and another three were taken after equilibration at each 10° C cooling interval. After dilution to 10 mL with mobile phase in a volumetric flask, a single injection of each sample was run through the column.

Three standard solutions of varying known concentrations were run through the HPLC system in order to form an HPLC calibration curve to be used in the calculation of the sample concentrations. The second standard was injected in triplicate, and verified the error in the method to be approximately 1%. The concentrations of the samples determined by HPLC were then compared to the concentration profiles established by the kinetic model. The results of this validation are shown in Figure 15.

The concentration profile of ASA predicted by the model falls within the majority of the error bars, suggesting that the estimates made by the kinetic model fitting are reasonable. There is a great deal of variability between the individual sample concentrations taken from the reaction mixture. Observations of the mixture showed that despite allowing time for the solid

particulate matter to settle to the bottom of the reaction vessel, the solution itself was still slightly turbid. This indicated that some ASA solid particles remained suspended in the solution when the aliquot was taken, explaining the variability between the samples. It was not practical to filter the aliquots taken from the reaction mixture because dissolved ASA would rapidly precipitate from the saturated solution on the slightly cooler filter. Also, the sampling step at 25°C was missed due to a mistake by the experimenter, resulting in no validation points at approximately 200 minutes.

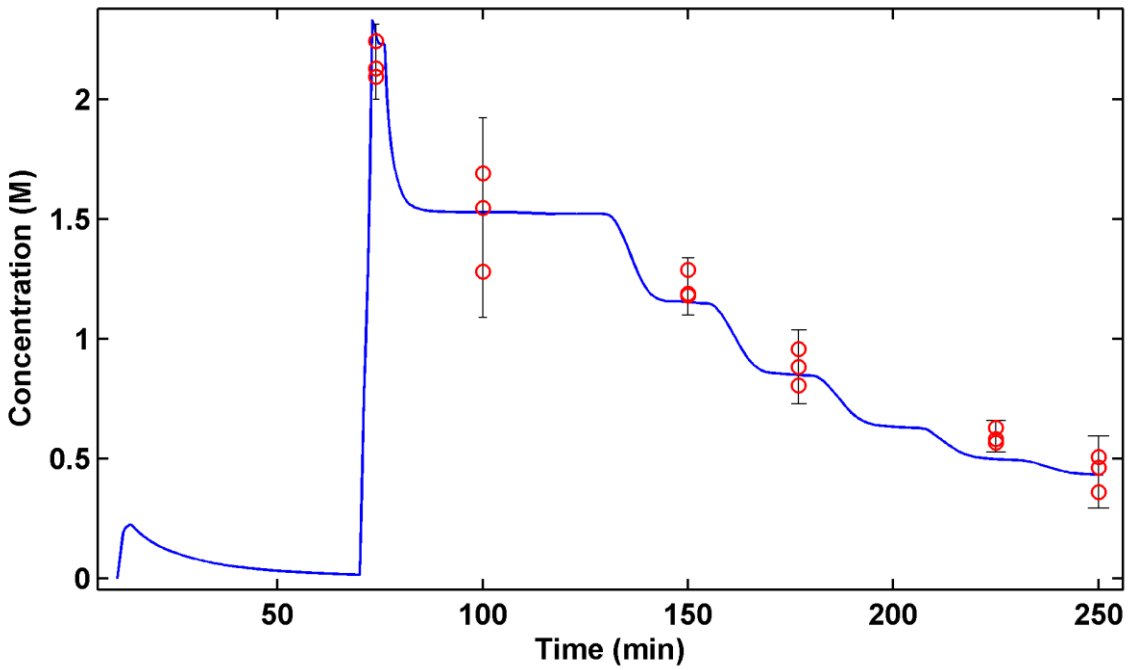

Figure 13. Validation of the concentration profile from the kinetic model fitting. The blue line is the concentration profile of ASA as determined by the model fitting. The red circles indicate the concentrations of the samples taken from the reaction mixture as determined by the HPLC measurements. Each plateau in the blue line between approximately 80 and 250 minutes indicates a temperature step 55°, 45°, 35°, 25°, 15°, and 5°C. There is no sample at 25°C, however, due to a mistake by the experimenter.

3.5. Conclusions

This work has established a kinetic model fitting algorithm that has the ability to accurately predict changes in concentration and measured absorbance of reaction systems that include dissolution, reaction, and crystallization steps. The method utilized an ATR-UV/Vis spectroscopy method to measure the absorbance of the solution phase of a complex reaction mixture. These measurements were then processed using an NGLM non-linear optimization method in conjunction with the numerical integration of a set of ordinary differential equations used to predict the changes in concentration for each component of the mixture as a function of time. This process resulted in an accurate prediction of both the spectral profile, demonstrated by the low values of *ssq*, and the concentration profile, confirmed by the HPLC validation measurements.

The modeling method presented here is very flexible, and could be applied to any spectroscopic method where there is a linear relationship between absorbance and concentration. The robustness and ease of implementation demonstrate the potential usefulness of this technique in a production setting, and the knowledge required to build a kinetic model for any reaction system will demonstrate an accurate understanding of the fundamental reaction steps as well as important kinetic parameters for ensuring the safety and efficiency of batch reaction processes in slurries.

4. Kinetic Hard Modeling of Batch Slurry Reactions

Summary:

The use of slurry mixtures in chemical and pharmaceutical manufacturing processes is common due to the advantages that this method provides. Kinetic modeling of large scale batch reactions has been shown to be an excellent tool in on-line batch reaction monitoring [15, 17, 27, 31, 32]. To date, little work has been done in modeling slurry reactions. Presented here is a kinetic modeling method for a commercially relevant slurry reaction that produces a solid suspension of the product. The model was built using near infrared (NIR) diffuse reflectance measurements taken by a submersible fiber-optic probe inside of a jacketed reactor vessel. Measurements were confirmed by off-line high performance liquid chromatography (HPLC) analysis with samples taken from a recirculation loop, and using focused beam reflectance measurement (FBRM) measurements to observe the product precipitation event. The system chosen was the reaction of a heterocycle triazine suspended in xylene with an isocyanate to form a metsulfuron methyl product precipitant.

KEY WORDS: Kinetic modeling; Spectroscopy; Slurries; Metsulfuron methyl; Nonlinear fitting

4.1. Introduction

The manufacturing of chemical and pharmaceutical products has greatly benefitted from the use of slurry mixtures in the production process. There are many advantages to using slurries; for instance, the production of a product that is simply suspended in a liquid solvent is

much easier to separate than a liquid product mixed with a liquid solvent. Simply drying the product instead of proceeding through a series of separation steps saves the manufacturer time and money. Also, depending on the situation, the amount of solvent used to suspend the materials can be minimized and more easily recycled for use in subsequent batches, which saves the manufacturer on cost of materials. It is for reasons such as these that the use of slurries in industrial reactions is common. However, batch reaction monitoring becomes more difficult when the materials being measured are in more than one phase.

Modeling of batch reactions in industry is typically done using a Partial Least Squares (PLS) method. However, these methods often require extensive and costly calibration data sets and may not be very robust to small modifications in product formulation. Kinetic modeling, on the other hand can be a more robust system that can compensate for changes in the experimental protocol as long as the appropriate mathematics have been added to the model set-up. For instance, if changes in reactor temperature are frequent, as long as the appropriate calibration has been added to the kinetic model parameters, then the modeled data should reflect the temperature changes, even in real time. If the mathematics in the kinetic model accurately represents the mechanisms of the reaction itself, then the model should be able to approximate a set of spectra that accurately reflects the experimentally measured data. A tool such as this is beneficial in industry for its ability to detect process upset errors in real time. For example, if the measurements from a production batch do not fall within an acceptable range predicted by the model, then the error can be noticed before the batch reaches the product testing stages. An error that is spotted early could even potentially be rectified. If there were a

mistake in the initial charge of starting materials, the batch mixture could be adjusted by the addition of reactants that would rectify the error and prevent the waste of time and materials.

Presented here is a functional kinetic model for a commercially relevant slurry system. The model characterizes the dissolution of a heterocycle triazine slurry that is suspended in xylene, its reaction with an isocyanate solution that is pumped in, and the subsequent precipitation of the metsulfuron methyl product.

4.2. Theory

Kinetic models are made up of a series of rate law equations that are used to build ordinary differential equations (ODEs) necessary to construct concentration profiles for all species present in the reaction system. Initially, certain values, such as the reaction rate constants, are unknown due to the fact that they vary by system and initial conditions. In order to obtain these values, a nonlinear optimization of the parameters must be performed to estimate them. Once they have been calculated, the concentration profiles should reflect the actual changes in concentration for each species present in the reaction and can be used to calculate the model fit. A tutorial for the kinetic model fitting process is described by Puxty [6], and will only be summarized here.

4.2.1 Building Concentration Profiles

The construction of concentration profiles is dependent on the use of a series of ODEs that establish the changes in concentration for each component in the system as a function of

time. In order to create the ODEs, however, the reaction mechanisms of the system must be known. These mechanisms are necessary to form the rate laws for each reaction and the ODEs are calculated based on these. A concentration profile that accurately portrays the changes that the system undergoes is necessary to establish a good model fit, so these rate laws and ODEs must describe the data as accurately as possible.

Construction of the ODEs can be quite simple, even if the reaction is somewhat complex. For instance, consider a two-step reaction mechanism:

$$\mathrm{A} + \mathrm{B} \xrightarrow{k_1} \mathrm{C} \tag{4-1}$$

$$2\mathrm{C} \xrightarrow{k_2} \mathrm{D} \tag{4-2}$$

The rate laws for these reactions can easily be established.

$$r_1 = k_1[\mathrm{A}][\mathrm{B}] \tag{4-3}$$

$$r_2 = k_2[\mathrm{C}]^2 \tag{4-4}$$

The rates of change for each component of the reaction, A, B, C, and D, are established by these rate laws and are combined in the ODEs.

$$\frac{d[\mathrm{A}]}{dt} = \frac{d[\mathrm{B}]}{dt} = -r_1 \tag{4-5}$$

$$\frac{d[\mathrm{C}]}{dt} = r_1 - 2r_2 \tag{4-6}$$

$$\frac{d[\mathrm{D}]}{dt} = r_2 \tag{4-7}$$

In order to calculate the concentration at any given moment, these differentials must be integrated with respect to time. Unfortunately, for such a large and complex data set, this is impossible to do explicitly. For this reason, a numerical integration method must be relied upon to calculate the concentration profiles. In this work, the fourth order Runge-Kutta method of numerical integration is used [34].

4.2.2 Calculating the Residuals

In order to establish how well the modeled concentration profiles fit the experimental data, an estimation of the model estimated spectra must be made for comparison. This estimated set of spectra is calculated using a restatement of the Beer-Lambert law:

$$\mathbf{Y}_{\mathrm{calc}} = \mathbf{CA} \tag{4-8}$$

Where $\mathbf{Y}_{\mathrm{calc}}$ is the estimated set of spectra, **C** is a matrix containing the concentration profiles for each component of the reaction, and **A** is a matrix containing the molar absorptivity for

each component. Because the matrix **A** is also unknown, it must be calculated using the calculated concentration profile and the measured experimental spectra.

$$\mathbf{Y} = \mathbf{CA} \Rightarrow \mathbf{A} = \mathbf{C}^{+}\mathbf{Y} \tag{4-9}$$

If **A** is replaced within the equation, it can be shown that this value is not necessary to compute the estimated spectra.

$$\mathbf{Y}_{\text{calc}} = \mathbf{CC}^{+}\mathbf{Y} \tag{4-10}$$

A matrix of residuals **R** is computed by taking the difference of **Y** and $\mathbf{Y}_{\text{calc}}$.

$$\mathbf{R} = \mathbf{Y} - \mathbf{Y}_{\text{calc}} \tag{4-11}$$

In order to establish how well the modeled spectra fit the experimental spectra, the sum of squares of the residuals is calculated.

$$ssq = \sum r_{ij}^{\ 2} \tag{4-12}$$

In the case that the two were a perfect match, the value of *ssq* would be equal to the measurement error in the experiment.

4.2.3 Nonlinear Optimization of Parameters

As previously mentioned, it is very unlikely that certain values, such as the reaction rate constants, are known when computing the concentration profiles. Fortunately, there are methods that can be used to optimize these values and give a close approximation to their true values. The method that is used here is the Newton-Gauss-Levenberg-Marquardt (NGLM) algorithm [20, 21]. This routine requires initial guesses for each of the unknown experimental parameters. Using these initial guesses, the modeled spectra are computed and the value for *ssq* is calculated. The algorithm then goes through a series of iterations wherein a shift for each parameter is calculated and a new set of model spectra is calculated. This is done repeatedly until the value of *ssq* converges.

4.3. Experimental

A series of three batch reactions were conducted at Stine-Haskell Research Center in Newark, DE. In-situ NIR reflectance measurements were collected for all batches. The same chemical conditions, experimental protocol and process conditions were used for all batches. In this paper, the slurry-based synthesis of Metsulfuron Methyl (see Figure 18), an herbicide manufactured by E.I. DuPont was studied. The studies included the chemical coupling reaction and the dissolution of metsulfuron methyl in xylene. The sulfonylurea coupling reaction is a

challenging system for reaction monitoring because one of the reactants and the product is only sparingly soluble in xylene, being present in both the solid and liquid phases of the slurry.

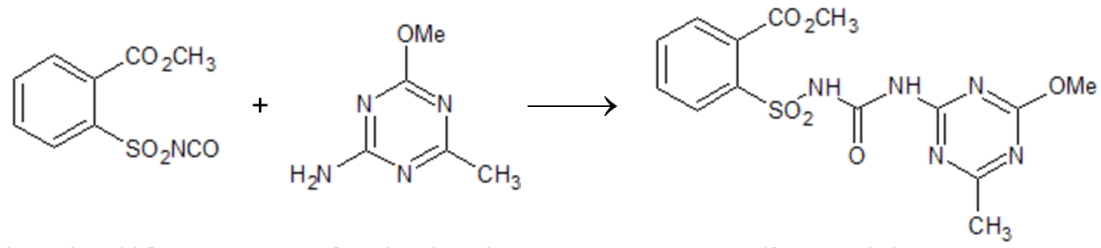

benzoic acid 2-[(Isocyanato)sulfonyl]-methyl ester

2-amino-4-methoxy-6-methyl-1,3,5-triazine

metsulfuron methyl

Figure 14. Sulfonylurea coupling reaction

4.3.1 Reactor and Apparatus Setup

The batch reactions reported in this paper were performed in a custom jacketed 1000 mL reaction vessel made at Stine-Haskell Research Center. As shown in Figure 17, the reactor and lid were specifically designed to accept an NIR reflectance probe, an overhead stirrer, a thermocouple, an FBRM probe (not shown), and an additional opening for the recirculation tube. The reactor jacket was thermostated using a heater/chiller oil bath. A calibrated balance and a peristaltic pump were used for isocyanate reagent delivery.

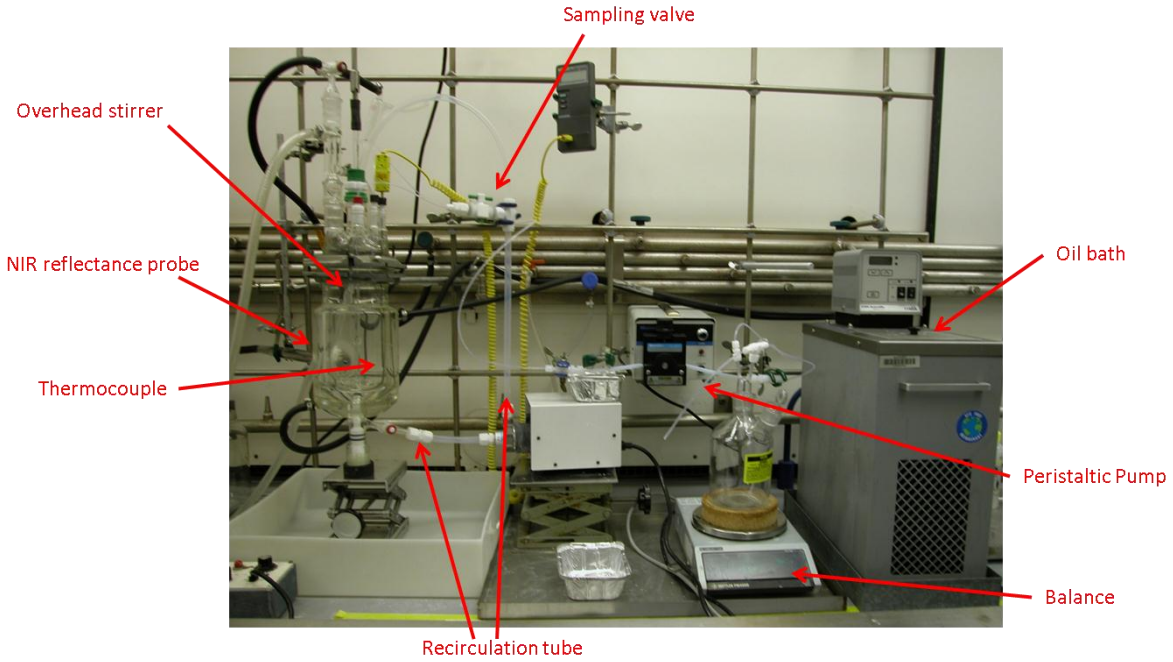

Figure 15. A picture of the lab-scale jacketed reactor and apparatus setup.

Before a batch reaction was initiated, the jacket temperature was set to a precisely controlled constant value of 85°C. The batch temperature was monitored using a calibrated thermocouple in the reactor.

4.3.2 Spectroscopic Instrument and Data Acquisition

NIR measurements were collected using a FOSS NIRSystems (Silver Spring, MD) model XDS Process Nema 4X monochromator in the 850-2200 nm regions, and a diffuse reflectance fiber optic probe (FOSS, 1.5 m, ½" OD x 12", sapphire lens). NIR spectra were measured at a rate of 1 per second. A total of 10 were averaged at every 30 second interval using Vision software designed by FOSS NIRSystem. For all batches, an internal reference spectrum was measured before each run.

4.3.3 Experimental Protocol

The sulfonylurea coupling reaction was carried out in a 1000 mL jacketed glass reactor. The reactants were 2-amino-4-methoxy-6-methyl-1,3,5-triazine (reagent A, $C_5H_9N_4O$, molecular weight 140.14, CAS 1668-54-8) and benzoic acid 2-[(Isocyanato)sulfonyl]-methyl ester, (reagent B, $C_9H_7NO_5S$ in $C_8H_{10,}$ molecular weight 241.2, DuPont) and the product was Metsulfuron Methyl (product P, molecular weight 381.4, CAS 74223-64-6). Both A and P have a very limited solubility in xylene (C_8H_{10}, molecular weight 106.16, CAS 1330-20-7). As reagent B is sensitive to moisture and water, and also harmful, it was quenched with isopropyl alcohol to form a derivative form of B, benzoic acid, 2-(((((1-methyl ethoxy)carbonylamino))sulfonyl))-methyl ester, (CAS 140617-87-4) when it was needed for calibration purposes.

The reactor was initially charged with 750 mL xylene solvent and 103 g of A at 85°C. B was dissolved in xylene and four additions of this solution (115 g of B per addition) were delivered via peristaltic pump. Each addition of reagent B corresponded to a quarter of the moles required for complete reaction, i.e. 25% of reaction (addition 1). After an equilibration time of 20 min, triplicate slurry samples were taken from the reaction mixture and analyzed by HPLC to validate results obtained by NIR spectroscopy.

Figure 18 shows the HPLC elution order for A, P, and the derivative form of B at 230 nm using a gradient method (water and acetonitrile) [45].

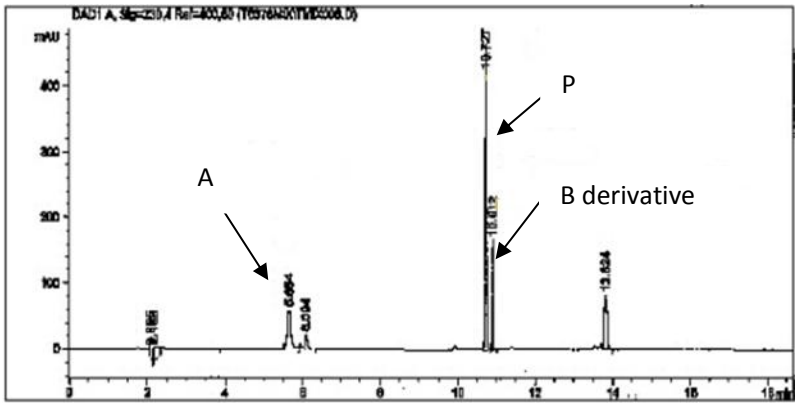

Figure 16. HPLC chromatogram showing the elution order of A, P and the derivative for of B at 230 nm using a gradient method. Column: Agilent Zorbax Eclipse C-18 (25 cm x 4.6 mm, 5um), temperature: 40 °C, injection volume: 10 uL, flow rate: 1.5 mL min^{-1}

Several different sampling techniques were tested, to ensure sufficient precision and reproducibility. In order to determine the minimum sample size that did not disturb the course of the reaction but was representative of the batch, two sampling techniques were compared. Sampling method (1), which only used a 20 µL slurry sample, was compared with sampling method (2), which used a 3.5 mL slurry sample. The reproducibility of triplicate aliquots was approximately the same for both sampling methods in terms of standard deviation, thus sampling method (1) was used in subsequent work.

4.3.4 Partial Least Squares Calibration

Before beginning the kinetic modeling of this system, it was confirmed that NIR reflectance measurements would be suitable for quantitative estimation of concentration profiles in a consistent manner from batch to batch. NIR reflectance measurements of a slurry mixture can yield inconsistent results due to variation in the reflectance signal attributed to differences in the light absorption and light scattering properties from batch to batch. A partial

least squares (PLS) calibration was performed to ensure that a calibration developed using one batch could be used to predictor the concentration profiles for another. A description of PLS calibration and prediction can be found in the literature, so only a brief summary of its use is provided here [7, 46-48].

To begin, a PLS calibration was performed on individual batch data sets. Each batch was run by adding a precisely measured amount of reagent B (isocyanate solution) to a precisely measured amount of reagent A (triazine) suspended in xylene. Samples were taken from the reactor vessel at specified points in time and the concentrations at those intervals were determined using HPLC analysis of each aliquot. The goal of PLS calibration was to relate the measured NIR reflectance spectra to the offline HPLC concentration information. Once the PLS calibration is established at the points in time where offline HPLC data is available, the PLS calibration can be used to estimate (interpolate) the concentration profiles of the reactant and product for an entire batch. The results from one such analysis are displayed in Figure 19. In Figure 19, a PLS calibration developed using a batch #1 run on 5/13/2010 was used to estimate the concentration profiles of a batch #2 run on 6/17/2010. Aliquots acquired from batch #2 were assayed by HPLC and plotted in Figure 19 for comparison with the PLS results. As can be seen in the plot, the estimate concentration profile and the HPLC concentrations agree, demonstrating that NIR reflectance measurements are useful for quantitative characterization of these slurry batch reactions.

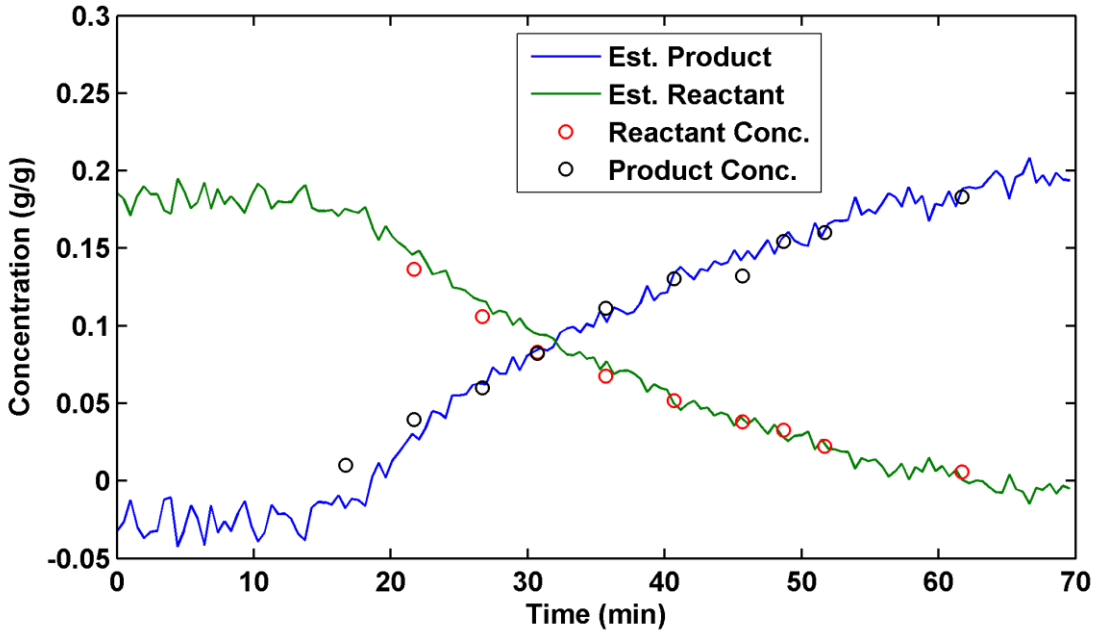

Figure 17. PLS calibration. Lines indicate the estimated concentrations of the reactant and product for batch #2 based on the calibration from batch #2. Circles indicate the concentration determined by HPLC.

4.3.5 Kinetic Models for Slurries and Numerical Integration

In order to fit a kinetic model, it was necessary to construct a system of Ordinary Differential Equations (ODEs) that represent a given reaction mechanism. In this paper, the system of ODEs used is shown in Equations 4-17 through 4-21. Equations 4-13 through 4-14 describe the reactions of reagent A with reagent B producing the product P in a batch reactor. Additional terms were required for reagent flow-in conditions used in a fed batch reactor.

$$\mathrm{A_s} \xrightarrow{k_1} \mathrm{A} \tag{4-13}$$

$$\mathrm{A} + \mathrm{B} \xrightarrow{k_2} \mathrm{P} \tag{4-14}$$

Equation 4-13 represents the dissolution process where the starting reagent A, a solid material, went from solid form A_s into solution form *A* after it was added into xylene, where k_1 is the dissolution rate constant. Equation 4-14 represents the sulfonylurea coupling reaction, where the dissolved form of A reacts with reagent *B* to form product *P*, where k_2 is the coupling reaction rate constant.

$$r_1 = k_1(C_A - C_{Asat})^d \tag{4-15}$$

$$r_2 = k_2 C_A C_B \tag{4-16}$$

From Equations 13-14, we constructed two rate laws (Equations 4-15 through 4-16) where r_1 and r_2 represent the rate of dissolution and the rate of the coupling reaction, respectively, k_1 and k_2 are the corresponding rate constants, C_A is the dissolved concentration of A in the bulk solution, C_{Asat} is the solubility of A, C_B is the B concentration, and *d* is the rate order of dissolution. The kinetic model was then translated into a system of Ordinary Differential Equations (ODEs), (Equations 4-17 through 4-21) which were numerically integrated resulting in the *nc* concentration profiles in **C**.

$$\frac{dV}{dt} = F \tag{4-17}$$

$$\frac{dC_{As}}{dt} = -r_1 - \frac{C_A}{V} F \tag{4-18}$$

$$\frac{dC_A}{dt} = r_1 - r_2 - \frac{C_A}{V}F \tag{4-19}$$

$$\frac{dC_B}{dt} = -r_2 + \frac{C_{Bin} - C_B}{V}F \tag{4-20}$$

$$\frac{dC_P}{dt} = r_2 - \frac{C_P}{V}F \tag{4-21}$$

In Equations 4-17 through 4-21, F is the flow-in rate (L/min) of solution B, V is the total volume of the slurry (L), C_{As} is the undissolved concentration of A (mol/L), C_B is the concentration of B inside the reactor (mol/L), C_{Bin} is the concentration of B in the reagent reservoir (mol/L), and C_P is the concentration of product P (mol/L).

4.4. Results and Discussions

At the beginning of the reaction, the reactor was charged with 750 mL xylene and 103 g of solid triazine heterocycle (A), which did not completely dissolve. During the reaction, the solid particles of A were suspended in xylene and was heated at 85 °C and agitated while a concentrated isocyanate solution (reagent B) was added via peristaltic pump to the reactor. At the end of an experiment, the mass of product P in the slurry was about 25-30% solid by weight (g/g) and the slurry had the consistency of a thick milk-shake.

Figure 20 shows the entire record of an experimental run. The upper panel of Figure 20 shows NIR reflectance data (log 1/R) for the sulfonylurea coupling reaction as a function of wavelength. In the bottom panel of Figure 20, the disappearance with time of the N-H overtone band at 2010 nm, uncorrected for baseline changes is shown and shaded bars show the times during which the peristaltic pump was turned on to deliver the isocyanate reagent solution. The NIR reflectance signal at 2010 nm increased when the first addition of B was introduced (until an elapsed time of 20 min). We suppose that reactant A, which was initially solid, dissolved as it was consumed by reactant B. A resulting baseline shift upwards in the log(1/R) signal at 2010 nm was observed due to the reduction in the particle density of reactant A in the slurry. At the same time the product, P, formed a supersaturated solution. After 20 min, the concentration of P exceeded the metastable supersaturated limit and spontaneously crystallized. The sudden increase in particle density due to precipitation of P resulted in a corresponding downward baseline shift in the log(1/R) signal at 2010 nm as shown by the steep drop or relaxation of the signal in Figure 19. Further relaxations, however were less pronounced than the first one, and were observed for the next three additions of B. A separate experiment was conducted to include an FBRM probe inside the reactor. FBRM measurements confirmed that supersaturation and an un-seeded nucleation and crystallization event occurred in the reactor during the first addition of reagent at the same point in time corresponding to the maximum in the log(1/R) signal at 2010 nm.

In order to evaluate the reproducibility of our experimental protocol and the reproducibility of the kinetic model fitting processes, two additional replicate batches were

performed but at a shorter time frame. This ensures the model was robust with respect to changes in the experimental time frame.

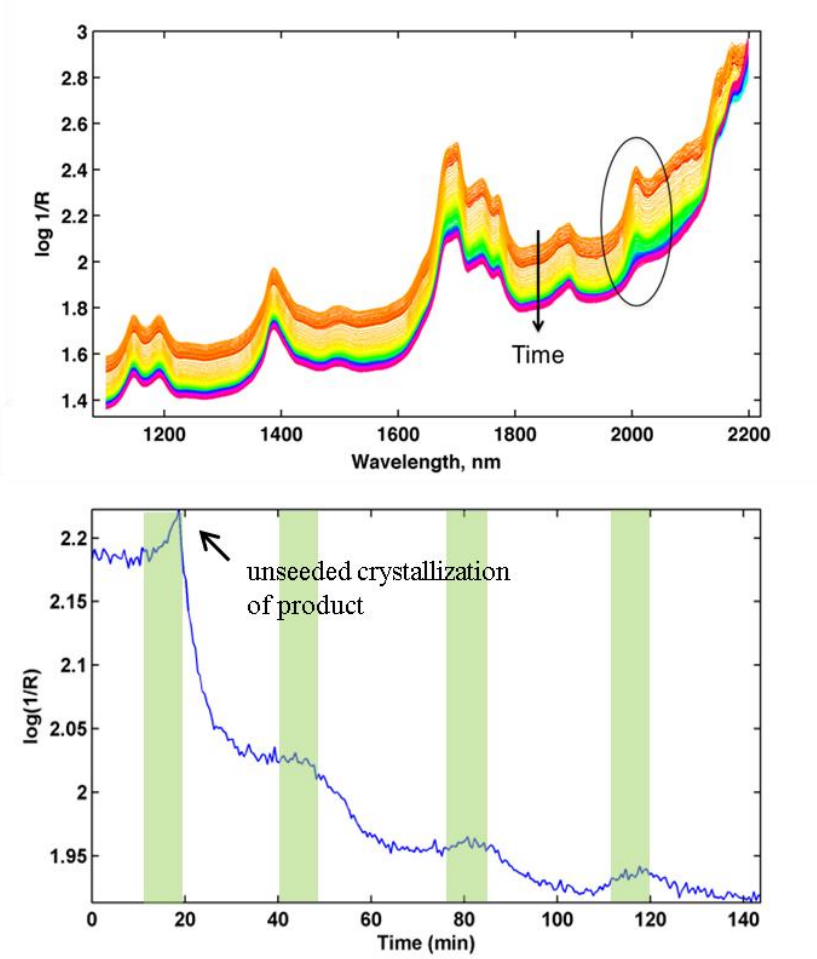

Figure 18. (Upper) NIR reflectance data (log 1/R) as function of wavelength, (bottom) time resolved NIR reflectance data at 2010 nm for the sulfonylurea coupling reaction involving four additions of B.

Preprocessing treatments were applied to the NIR reflectance spectra before being fitted with the kinetic model. NIR reflectance spectra were first treated with the Extended Multiplicative Scatter Correction (EMSC) technique[49], which models baseline offsets in near-infrared spectra as a combination of an offset, a function linear with wavelength and a function quadratic with wavelength. After baseline correction, the spectra were normalized to the mean spectrum in order to remove changes in path length effects.

Figure 21 shows the preprocessed near-infrared spectra used in the kinetic fitting process. The left panel shows the measured near infrared spectra as a function of wavelength, and the right panel shows the model estimated spectra as a function of wavelength. Good agreement can be seen to exist between the measured and modeled spectra.

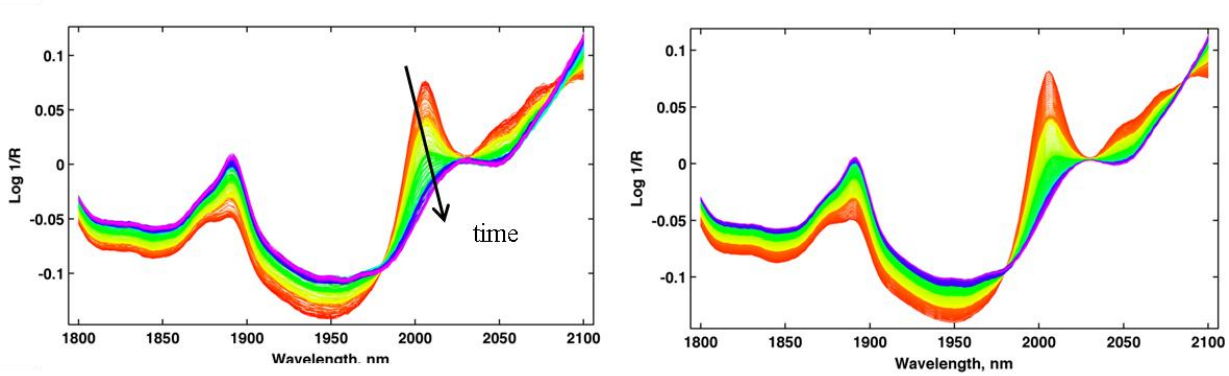

Figure 19. Comparison of the measured spectral data (left) with model estimated spectral data (right) as a function of wavelength to show the quality of fitting.

In these experiments, we assumed the slurries were well-mixed such that all particles of A and P were suspended relatively uniformly throughout the reactor vessel, inside the recirculation loop, and that the stirring rate was relatively constant. We also assumed the particle size distribution of the solid materials remained approximately the same throughout the experiment.

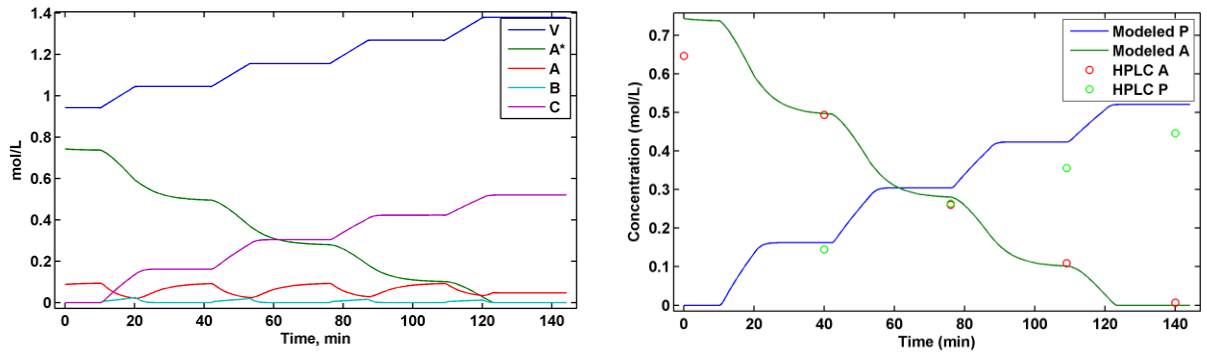

Figure 20. Comparison of the model estimated concentration profiles as a function of time. V is volume, A and A* are the dissolved and solid forms of A, respectively, B is reagent B, and C and P both represent the product P.

In the Figure 22, the left plot shows the model estimated concentration profiles. The blue continuous line shows the total volume (V), the green and red continuous lines shows the solid (A*) and liquid (A) form of A, respectively. The turquoise continuous line shows the flow-in profile for the isocyanate reagent (B), the purple continuous line shows the concentration profile of P (C). When B reagent was first introduced, it was consumed by the liquid phase of A and formed the product, P (C), immediately. The right plot shows the comparison of model estimated concentration profiles with HPLC data as a function of time for validation purposes. The green curve shows the model estimated concentration profile of A, the blue curve shows the model estimated concentration profile of P, and the red and green circles show the concentration of A and the concentration profiles of P measured by off-line HPLC, respectively.

Good agreement was observed between the off-line HPLC results (red circles) and the model estimated concentration of starting material (green curve) as a function of time; however, significant discrepancies were observed for the product. The source of error was most likely from the HPLC validation work, because we know the stoichiometry of the reaction and the initial concentrations of the reagents precisely. When running the protocol, in certain

batches, the contents of the container of reagent B were running low, and the reagent reservoir on the balance was tilted slightly. Therefore, the amount of mass delivered in the last addition may not be very accurate, and thus we used the estimated amount for the last addition. We know the calibrated pump was pumping at a constant speed and how much reagent pump delivered in the first three additions. Consequently, we took the average of first three additions and assumed that the pump continued to deliver the same amount for the last addition because it never actually ran dry.

Table 2. Kinetic model fitting results fitted with NIR reflectance data.

Parameters	**Batch A**		**Batch B**		**Batch C**		**Average**	**STD**	**RSD**
	Input	*Optimized*	*Input*	*Optimized*	*Input*	*Optimized*			
K_1	0.2000	0.5802	0.2000	0.1604	0.2000	0.2341	0.3249	0.2241	68.99
K_2	6.000	6.1261	6.000	26.55	6.000	64.94	32.54	29.86	91.78
A_{sat}	0.08800	0.06380	0.08800	0.09490	0.08800	0.07020	0.07630	0.01642	21.52
SSQ		0.1278		0.3310		0.3011	0.2533	0.1097	43.31

Table 2 shows the comparison of the kinetic model fitting results, obtained by fitted NIR reflectance measurements. For the purpose of this empirical model fitting process, reasonably satisfactory fitting results were obtained. The purpose of the model fitting process is not to determine fundamental constants in properties of dissolution or chemical reaction rates. Instead, the purpose is to develop an empirical model that gives accurate estimates of concentration profiles and a statistically sufficient phenomenological description of the batch process for monitoring and control.

4.5. Conclusion

In summary, we have developed a novel kinetic modeling strategy to monitor commercially relevant slurry reactions (i.e. dissolution and coupling reaction). NIR reflectance spectral data were measured using a fiber-optic probe inside of a jacketed reactor vessel. FBRM measurements confirmed the observation of the product precipitation event in the NIR diffuse reflectance spectra. In order to determine the kinetic parameters involved during the dissolution and coupling reaction processes, a simplified comprehensive global model describing these processes as a function of time was constructed and fit to the NIR measurements using MATLAB and nonlinear estimation methods. The parameters estimated in the model included dissolution and coupling reaction rate constants, and solubility of A in xylene at 85 °C. At the present time, the HPLC validation does not support the submission of Chapter 4 for publication of a journal article. Future work includes a careful analysis and kinetic modeling of batch data from May 2010 that has not been analyzed yet, and expanding the existing kinetic model by incorporating nucleation and crystallization processes. It is hoped that this will help improve the quality of fitting results.

4.6. Acknowledgement

All authors are grateful to the financial support from the National Science Foundation (NSF) under Grant Number CHE-0750287, Grant Opportunities for Academic Liaison with Industry (GOALI) and the E.I. DuPont de Nemours and Co., Inc., Crop Protection Products and Engineering Technologies. Chun Hsieh thanks Dr. Rich Davis, Dr. David Cho, David Bailey, Steve

Platz, and Kevin Day and for their assistance for the experimental set up and technical supports at Stine-Haskell Research Center.

4.7. Notations

C_A dissolved A concentration (mol/L)

C_{As} undissolved A concentration (mol/L)

C_{Asat} solubility of A (mol/L)

C_B B concentration in bulk solution (mol/L)

C_{Bin} B concentration in reagent reservoir (mol/L)

C_P P concentration in bulk solution (mol/L)

d dissolution rate order

F flow-in profile (L/min)

k_1 dissolution rate constant $L^{n-1}/(mol^{n-1}min)$

k_2 coupling reaction rate constant $L^{n-1}/(mol^{n-1}min)$

r_1 dissolution rate (mol/L/ut)

r_2 coupling reaction rate (mol/L/ut)

V total volume (L)

5. Conclusions

The work in this thesis has demonstrated the ability of a kinetic modeling system to accurately and robustly model different forms of reaction systems. As mentioned previously, work had been done on modeling dissolutions, crystallizations, and other chemical reaction processes, but prior work had been done to bring multiple processes together into one cohesive model system.

In Chapter 3, a relatively simple and well-known model system was analyzed by kinetic fitting, and these methods were able to accurately model spectra and concentrations as the system moved through simultaneous dissolution, reaction, and crystallization processes. In Chapter 4, these methods were again utilized to model an industrial slurry system using a different spectroscopic technique. The use of more than one spectroscopic technique and in more than one type of reaction system demonstrates the versitility of the kinetic modeling method.

There are several implications for industrial settings due to the fact that the technique has been shown to be flexible while maintaining robustness. In industry, kinetic models could be used to accurately monitor large scale batch reactions, ensuring quality and reproducibility of a product. Monitoring of these processes can be done currently using Partial Least Squares (PLS) methods; however, the same form of a kinetic model can be implemented repeatedly with different formulations of a product with few changes to the model's internal structure, whereas, with a PLS model, time-consuming and costly calibration data sets must be done to

establish a new model before it can be used. Use of a flexible model will save on the development time and cost of new or revised product formulations.

Kinetic modeling has proven to be a useful tool for recognizing what is taking place within a reaction system, and the work done here has further extended its usefulness by demonstrating its ability to model slurry systems and dissolution and crystallization phenomena simultaneously with reaction processes.

References

1. Nomikos, P. and J.F. MacGregor, *Monitoring batch processes using multiway principal component analysis.* AIChE Journal, 1994. **40**(8): p. 1361-1375.
2. Brereton, R.G., *Chemometrics: data analysis for the laboratory and chemical plant*2003: Wiley.
3. Nomikos, P. and J.F. MacGregor, *Multi-way partial least squares in monitoring batch processes.* Chemom. Intell. Lab. Syst., 1995. **30**(Copyright (C) 2012 American Chemical Society (ACS). All Rights Reserved.): p. 97-108.
4. Camacho, J., J. Pico, and A. Ferrer, *Multi-phase analysis framework for handling batch process data.* J. Chemom., 2008. **22**(Copyright (C) 2012 American Chemical Society (ACS). All Rights Reserved.): p. 632-643.
5. Gunther, J.C., J.S. Conner, and D.E. Seborg, *Process monitoring and quality variable prediction utilizing PLS in industrial fed-batch cell culture.* J. Process Control, 2009. **19**(Copyright (C) 2012 American Chemical Society (ACS). All Rights Reserved.): p. 914-921.
6. Puxty, G., M. Maeder, and K. Hungerbühler, *Tutorial on the fitting of kinetics models to multivariate spectroscopic measurements with non-linear least-squares regression.* Chemometrics and Intelligent Laboratory Systems, 2006. **81**(2): p. 149-164.
7. Gemperline, P., *Practical Guide to Chemometrics*2006: CRC/Taylor & Francis.

8. Gemperline, P.J., et al., *Chemometric characterization of batch reactions.* Proc. Annu. ISA Anal. Div. Symp., 1998. **31**(Copyright (C) 2012 American Chemical Society (ACS). All Rights Reserved.): p. 157-165.

9. Maeder, M. and Y.-M. Neuhold. *Kinetic modeling of multivariate measurements with nonlinear regression [in chemometrics]*. 2006. CRC Press LLC.

10. Gemperline, P., et al., *Calibration-Free Estimates of Batch Process Yields and Detection of Process Upsets Using in Situ Spectroscopic Measurements and Nonisothermal Kinetic Models: 4-(Dimethylamino)pyridine- Catalyzed Esterification of Butanol.* Anal. Chem., 2004. **76**(Copyright (C) 2012 American Chemical Society (ACS). All Rights Reserved.): p. 2575-2582.

11. Ma, B., et al., *Characterizing batch reactions with in situ spectroscopic measurements, calorimetry and dynamic modeling.* J. Chemom., 2003. **17**(Copyright (C) 2012 American Chemical Society (ACS). All Rights Reserved.): p. 470-479.

12. Yu, Z.Q., P.S. Chow, and R.B.H. Tan, *Application of attenuated total reflectance-Fourier transform infrared (ATR-FTIR) technique in the monitoring and control of anti-solvent crystallization.* Industrial & Engineering Chemistry Research, 2006. **45**(1): p. 438-444.

13. A.N. Saleemi, C.D.R., Z.K. Nagy, *Strategic Feedback Control of Pharmaceutical Crystallization Systems*, in *Chemical Engineering*2011, Loughborough University: Loughborough. p. 194.

14. Blandin, A.F., et al., *Kinetics identification of salicylic acid precipitation through experiments in a batch stirred vessel and a T-mixer.* Chemical Engineering Journal, 2001. **81**(1-3): p. 91-100.

15. Caillet, A., N. Sheibat-Othman, and G. Fevotte, *Crystallization of monohydrate citric acid. 2. Modeling through population balance equations.* Crystal Growth & Design, 2007. **7**(10): p. 2088-2095.

16. Cornel, J., C. Lindenberg, and M. Mazzotti, *Quantitative application of in situ ATR-FTIR and Raman spectroscopy in crystallization processes.* Industrial & Engineering Chemistry Research, 2008. **47**(14): p. 4870-4882.

17. Cornel, J. and M. Mazzotti, *Estimating Crystal Growth Rates Using in situ ATR-FTIR and Raman Spectroscopy in a Calibration-Free Manner.* Industrial & Engineering Chemistry Research, 2009. **48**(23): p. 10740-10745.

18. Nagy, Z.K., *Model based robust control approach for batch crystallization product design.* Computers & Chemical Engineering, 2009. **33**(10): p. 1685-1691.

19. Nagy, Z.K., M. Fujiwara, and R.D. Braatz, *Modelling and control of combined cooling and antisolvent crystallization processes.* Journal of Process Control, 2008. **18**(9): p. 856-864.

20. Levenberg, K., *A method for the solution of certain problems in least squares.* Quart. Applied Math., 1944. **2**: p. 164-168.

21. Marquardt, D.W., *AN ALGORITHM FOR LEAST-SQUARES ESTIMATION OF NONLINEAR PARAMETERS.* Journal of the Society for Industrial and Applied Mathematics, 1963. **11**(2): p. 431-441.

22. *MATLAB R2009a*. 2009; Available from: http://www.mathworks.com.

23. Hind, A.R., S.K. Bhargava, and A. McKinnon, *At the solid/liquid interface: FTIR/ATR — the tool of choice.* Advances in Colloid and Interface Science, 2001. **93**(1–3): p. 91-114.

24. Schlemmer, H. and J. Katzer, *ATR technique for UV/visible analytical measurements.* Fresenius' Z. Anal. Chem., 1987. **329**(Copyright (C) 2012 American Chemical Society (ACS). All Rights Reserved.): p. 435-9.

25. Reich, G., *Near-infrared spectroscopy and imaging: Basic principles and pharmaceutical applications.* Adv. Drug Delivery Rev., 2005. **57**(Copyright (C) 2012 American Chemical Society (ACS). All Rights Reserved.): p. 1109-1143.

26. Puxty, G., et al., *Modeling of batch reactions with in situ spectroscopic measurements and calorimetry.* J. Chemom., 2006. **19**(Copyright (C) 2012 American Chemical Society (ACS). All Rights Reserved.): p. 329-340.

27. Puxty, G., et al., *Multivariate kinetic hard-modelling of spectroscopic data: A comparison of the esterification of butanol by acetic anhydride on different scales and with different instruments.* Chemical Engineering Science, 2008. **63**(19): p. 4800-4809.

28. Skoog, D.A., F.J. Holler, and S.R. Crouch, *Principles of Instrumental Analysis*2007: Thomson Brooks/Cole.

29. Blanco, M. and I. Villarroya, *NIR spectroscopy: a rapid-response analytical tool.* TrAC, Trends Anal. Chem., 2002. **21**(Copyright (C) 2012 American Chemical Society (ACS). All Rights Reserved.): p. 240-250.

30. Kreyszig, E., *Advanced Engineering Mathematics*2011: John Wiley & Sons.

31. Puxty, G., et al., *Modeling of batch reactions with in situ spectroscopic measurements and calorimetry.* Journal of Chemometrics, 2005. **19**(5-7): p. 329-340.

32. Westerhuis, J.A., S.P. Gurden, and A.K. Smilde, *Spectroscopic Monitoring of Batch Reactions for On-Line Fault Detection and Diagnosis.* Analytical Chemistry, 2000. **72**(21): p. 5322-5330.

33. Simon, L.L., Z.K. Nagy, and K. Hungerbuhler, *Comparison of external bulk video imaging with focused beam reflectance measurement and ultra-violet visible spectroscopy for metastable zone identification in food and pharmaceutical crystallization processes.* Chemical Engineering Science, 2009. **64**(14): p. 3344-3351.

34. Press, W.H., et al., *Numerical Recipes in C: The Art of Scientific Computing*1992: Cambridge University Press. 1035.

35. Domb, A.J., *Quantitative analysis of mixtures of symmetric and mixed anhydrides.* Journal of Chromatography A, 1994. **673**(1): p. 31-35.

36. March, J., *Advanced organic chemistry: reactions, mechanisms, and structure*1992: Wiley.

37. Florey, K., *Analytical Profiles of Drug Substances, Vol. 3*1974: Academic. 579 pp.

38. Cornel, J., C. Lindenberg, and M. Mazzotti, *Experimental Characterization and Population Balance Modeling of the Polymorph Transformation of L-Glutamic Acid.* Crystal Growth & Design, 2009. **9**(Copyright (C) 2012 American Chemical Society (ACS). All Rights Reserved.): p. 243-252.

39. Garside, J., *Industrial crystallization from solution.* Chemical Engineering Science, 1985. **40**(1): p. 3-26.

40. Caillet, A., N. Sheibat-Othman, and G. Fevotte, *Crystallization of Monohydrate Citric Acid. 2. Modeling through Population Balance Equations.* Crystal Growth & Design, 2007.

7(Copyright (C) 2012 American Chemical Society (ACS). All Rights Reserved.): p. 2088-2095.

41. Higuchi, W.I., E. Nelson, and J.G. Wagner, *Solubility and dissolution rates in reactive media.* Journal of Pharmaceutical Sciences, 1964. **53**(3): p. 333-335.

42. Costa, P. and J.M. Sousa Lobo, *Modeling and comparison of dissolution profiles.* European Journal of Pharmaceutical Sciences, 2001. **13**(2): p. 123-133.

43. Atkins, P.W. and J. De Paula, *Élements of physical chemistry*2005: Oxford University Press.

44. Billeter, J., Y.-M. Neuhold, and K. Hungerbühler, *Systematic prediction of linear dependencies in the concentration profiles and implications on the kinetic hard-modelling of spectroscopic data.* Chemometrics and Intelligent Laboratory Systems, 2009. **95**(2): p. 170-187.

45. DuPont HPLC methods Y6266.200.01.BE, T.E., T6376.220.05.ES, 2000, 1999, 2004.

46. Ni, W.D., S.D. Brown, and R.L. Man, *Stacked partial least squares regression analysis for spectral calibration and prediction.* Journal of Chemometrics, 2009. **23**(9-10): p. 505-517.

47. Geladi, P. and B.R. Kowalski, *Partial least-squares regression: a tutorial.* Analytica Chimica Acta, 1986. **185**(0): p. 1-17.

48. Xu, Q.-S., Y.-Z. Liang, and H.-L. Shen, *Generalized PLS regression.* Journal of Chemometrics, 2001. **15**(3): p. 135-148.

49. Martens, H., J.P. Nielsen, and S.B. Engelsen, *Light scattering and light absorbance separated by extended multiplicative signal correction. Application to near-infrared transmission analysis of powder mixtures.* Analytical Chemistry, 2003. **75**(3): p. 394-404.